STUDY OF DRUG DELIVERY AND CELL ENCAPSULATION USING BIOCOMPATIBLE HYDROGEL

BY

FELICE CHENG

DISSERTATION

Submitted in partial fulfillment of the requirements
for the degree of Doctor of Philosophy in Electrical and Computer Engineering
in the Graduate College of the
University of Illinois at Urbana-Champaign, 2010

Urbana, Illinois

Doctoral Committee:

Professor Kyekyoon Kim, Chair
Professor William D. O'Brien, Jr.
Adjunct Professor Kuang-Chien Hsieh
Lecturer Hyungsoo Choi

ABSTRACT

Hydrogel particles encapsulating biomolecules or living cells are becoming an attractive means to mediate drug delivery or facilitate cell-based treatment of diseases. These particles are capable of maintaining drug stability/cell viability and providing specific drug release profiles. The selection of specific hydrogel and particle size depends on the administration routes, properties of the therapeutics and desired release profiles, and dictates the fabrication methods. We have chosen to design and fabricate hydrogel particles as a means to improve the efficacy of drug delivery utilizing mechanical, hydrodynamic and electric forces (precision particle fabrication (PPF) method and its modified scheme). Using such precision particles, we studied the drug release mechanisms that may help improve the design of new drug delivery vehicles.

Monodisperse gelatin microspheres, fabricated via the electric field assisted PPF method, allowed detailed analysis of drug release without uncertainties ascribable to nonuniform particles. The results from this analysis, including zeta potential, particle swelling ratio, and intraparticle drug distributions, led to a release model, based on the reaction-diffusion and Michaelis-Menten kinetics. This model elucidates the effect of glutaraldehyde, a cross-linking agent, on release profile in terms of the initial drug distribution, diffusivity, degradation rate of gelatin and its ability to form polyionic complex with the drug. By measuring the drug diffusion constant and initial intrapaticle drug distribution in advance, the

model can predict the drug release and serve as a design tool for certain drug delivery scenarios.

Hydrogel particles with peptide coating were developed as a vehicle for targeted delivery. The proposed drug delivery vehicle contains three main components: (1) anticancer drug, (2) targeting peptide, and (3) drug carrier. In this study, the peptide was used to target Cathepsin D that is overexpressed by breast cancer cells. Gelatin microspheres were utilized as drug carriers which immobilized doxorubicin, an anticancer drug. Uniform gelatin particles (30 μm in diameter, dry) were fabricated via the electric field assisted PPF method to optimize the drug loading efficiency. The particles suitable for intravenous injection (<10 μm, dry) were fabricated by increasing the electric field strength. The results of the release study and chemotherapy on cancer cells, performed in collaboration with Prof. Logan Liu's group, confirmed that the use of peptide coating as a targeting moiety substantially enhanced the efficacy of chemotherapy, which would alleviate the adverse effect of chemotherapy ascribable to systemic distribution of chemotherapeutics.

Alginate microspheres/microcapsules of precisely controlled size and size distribution were employed for cell encapsulation which could be utilized in cell-based therapy and artificial organs. Cell viability was shown to remain intact after the encapsulation. The cross-linking of alginate with calcium ion involved the motion of both alginate molecules and calcium ions. The observation of significant size shrinkage from alginate microdroplets to microspheres indicated a junction-zone mode of the cross-linking process. A particle sorting scheme

combining optical detection and electric deflection was developed to deflect out capsules empty of cells and increase the yield in cell encapsulation. This may contribute to reducing the volume of microcapsules required for transplantation and make clinical application more practical.

In summary, we have demonstrated the flexibility and practicality of the modified PPF method in producing precision hydrogel particles and the suitability of these particles for applications involving their applications for controlled drug delivery and tissue engineering.

ACKNOWLEDGMENTS

Thanks be to God for His love and guidance through my life.

I wish to thank my advisers, Professor Kyekyoon Kim and Professor Hyungsoo Choi, for their enormous guidance, encouragement and support in this research. They advise like good parents with tremendous love and support which sets a role model for mentoring. I would also like to thank my Ph.D. committee members, Professors William D. O'Brien and Kuang-Chien Hsieh, for their guidance. I am also grateful to Dr. Young Bin Choy, who mentored me in microsphere fabrication and *in vitro* drug release study.

I would like to thank all members of the Thin Film and Charged Particle Research Laboratory for their help and support. Their amiability and friendship will never be forgotten. Especially, I would like to thank Hee Kyung, Anil Kumar, Leslie Hwang, Inyong Kim, Jangho Kim, Phil Heil and Wenhua Gu for their contributions to or insightful discussions about the present work.

I would like to thank my family for their support for whatever decision I made in my life. I thank my best friends, Angel Chen and Edward Chen, for their encouragement and friendship. Thanks also go to members of my Vineyard bible study group for their continuous love and prayers which bring me closer to God.

This work was financially supported by the University of Illinois and the Linda Su-Nan Chang Sah Doctoral Fellowship.

TABLE OF CONTENTS

CHAPTER 1

INTRODUCTION

1.1 Hydrogel in drug delivery and tissue engineering

Progress in biotechnology has facilitated the discovery of new therapeutics involving peptides, proteins, cells and other potent/fragile drugs. For example, there are more than 40 marketed peptides or proteins worldwide including insulin, vancomycin, oxytocin and cyclosporine [1-4]. Cell-based therapies, utilizing artificial organs and delivery of genetically engineered cells, have been investigated for the past decades, and some are currently undergoing clinical trials [5]. While more understanding of pharmaceutics is established providing new hopes of cures for many currently untreatable diseases, achievement of high efficacy in the delivery of the pharmaceutics still has room for much improvement.

Polymeric particles have attracted considerable attention in controlled drug delivery due to their stability, versatility for surface modification [6,7] and potential for achieving different drug release characteristics [8-10]. These delivery vehicles could provide long-term drug delivery, resulting in less frequent administration, which is a key to successful therapy for brain traumata or diseases in which multiple doses might not be feasible, thus reducing necrosis induced by repeated injection. The polymeric particles could also be modified on the surface so that the drug release may be triggered at the specific sites or in

certain environments [6,7] thus preventing systemic distribution of therapeutics. In addition to applications involving drug delivery, recent research also reported the use of polymeric particles as a means for providing immunoprotection for the transplanted cells [11], establishing a specific tissue culture microenvironment regulating stem cell differentiation [12,13] or increasing the viability of cultured cells [14]. Of various polymers, natural hydrogels have demonstrated excellent compatibility with tissue, good control of solute permeability, ability to be injected directly into the affected areas [15,16] and non-toxic or mildly toxic processing conditions, which maintain the functionality of biomolecules or viability of encapsulated cells.

Particle size control has several important implications for controlled drug delivery and cell encapsulation such as drug release rate and viability of encapsulated cells [14]. The rate of drug diffusion and degradation of the polymer matrix strongly depends on the surface-to-volume ratio of the particles, which is a function of particle size. Besides, the biodistribution of the particles inside the body is influenced by their size. Rigid particles with a diameter of 6-10 μm were reported to be trapped in lungs (more than 84%), whereas the majority of those with a diameter less than 4 μm were found in the reticuloendothelial system (RES) [17]. Also, particles of 100-1200 nm in diameter might be used for cancer-targeting delivery via the enhanced permeability and retention (EPR) effect ascribable to the loose structure of tumor microvessels. Therefore, a desired drug release behavior which depends on drug release rate and biodistribution of drug carrier cannot be achieved without controlled particle size and size

distribution. Besides, investigation of processing parameters on drug release behavior could not be achieved either because of uncertainty due to the wide size distribution of particles. In tissue engineering, the optimal size of microcapsules encapsulating cells varies. For example, Dufrane et al. showed that pig islets in alginate microcapsules of 635 μm in diameter survive up to six months after transplantation without immunosuppression [18]. On the other hand, it was suggested that hepatocytes in the center of alginate microcapsules larger than 400 μm might not maintain their viablity due to limited diffusion of oxygen and nutrients [19]. Dying cells not only provide no therapeutic effects but might also cause adverse effects such as inflammatory responses. Besides, size reduction in capsules usually increases the percentage of inadequately encapsulated cell aggregates while islet cell aggregates show superior survival and functionality [20]. Therefore, fabrication of particles in controlled size and size distribution is crucial for both drug delivery and cell encapsulation.

In the next section, we will review some of the most significant types of protocols for fabricating hydrogel particles.

1.2 Fabrication of hydrogel-based particles

Within the past decades, a multitude of protocols have been developed and reported, using synthetic or natural hydrogels to fabricate biopolymeric particles for drug delivery and cell encapsulation. Here the fundamentals of emulsion, desolvation, mechanical vibration, spray drying and co-axial air jet methods are reviewed.

1.2.1 Emulsion

Emulsion method has been utilized for fabrication of polymeric particles from different materials. Hydrogel particles can be produced using simple water-in-oil emulsion. Despite a multitude of emulsion techniques described in the literature, all of them suffer from certain shortcomings, such as low yields (<30%) or broad size distributions probably due to the lack of effective emulsifiers or surfactants. In addition, high energetic methods such as ultrasound, high-pressure or high-speed homogenization have to be applied to achieve adequate particles sizes. These apparatus are expensive and the process might lead to denature of materials because of the heat generated during the process. Furthermore, purification to remove the toxic organic phase and remaining emulsifier is usually complex and tedious. Finally, the use of toxic organic phase or emulsifier makes this method inadequate for encapsulation of biomolecules or living cells.

1.2.2 Desolvation

Desolvation is a process of removal or dissociation of the solvent from a solution which is commonly used to purify or concentrate biomolecules such as DNA, RNA, proteins and polysaccharides from an aqueous solution. The main concept for such desolvation methods, sometimes referred to as precipitation, is to reduce the solubility of the solute in the solvent which can be achieved by

addition of neutral salt as salting-out agents [21], hydrophilic polymers such as dextran or polyethylene glycol [22] or miscible organic solvents [23], and by adjustment of the solution pH to the isoelectric point of the material [24]. The desolvation method is appropriate for the preparation of particles composed of charged polymer with a defined molecular weight. However, for natural polymer with a wide range of molecular weight the method lacks reproducibility and homogeneity of the resulting particles. The obstacle might be resolved by eliminating the lower molecular weight fraction before the precipitation of particles, which leads to homogeneity of the particles [25]. Still, current protocols lack size control of particles and generally result in hydrogel particles smaller than 1 μm which significantly increase the drug release rate due to their high surface-to-volume ratio.

1.2.3 Mechanical vibration

Mechanical vibration on solution jet has been utilized to fabricate particles of different sizes. Lord Rayleigh first found that the most unstable disturbance wave imposed on a jet surface resulted in the break-up of the jet into uniform droplets. With the wave of an optimal wavelength, droplet radius is typically 1.9 times the jet radius. Although disturbance of other wavelengths might produce uniform droplets, jet size and therefore nozzle opening are still the limiting factors in producing small particles. The precision particle fabrication method developed by Kim et al. has been applied to resolve the above problems and to fabricate polymeric particles of sizes much smaller than the nozzle opening. During the

process, polymer solution forms a jet of a diameter smaller than the nozzle opening due to the hydrodynamic forces of the surrounding immiscible solution. The jet is further broken into uniform droplets by mechanical forces and the droplets become uniform particles after drying. The concurrent use of mechanical and hydrodynamic forces allows this method to be less limited by nozzle dimension or solution viscosity. Sizes of hydrogel particles are still confined to micro scales, usually larger than 50 μm after swelling when administered into living tissue, because of jet instability, especially when the jet diameter goes below 20 μm.

1.2.4 Spray drying

Spray drying is a method of producing dry powders from a solution via three processing stages: atomization, evaporation in air and collection of dry product from the exit air [26]. Atomization determines the size and size distribution of the particles, which are the single most crucial factor in the process. The droplet size establishes the available heat transfer surface area, and thus the drying chamber design is influenced by the choice of atomizer. Spray drying provides effective control of product properties and quality, and high production rate in continuous operation, and is thus suitable for heat-sensitive materials. Among all atomization techniques, electrospray might be the most important technology; it employs high voltage to disperse the solution, which is supplied through a nozzle. Various waves on the surface of the jet lead to the formation of droplets which are subsequently dispersed due to Coulomb repulsion. Particle

size resulting from electrospray of aqueous solution is usually greater than a few hundred micrometers possibly due to the high conductivity of water.

1.2.5 Coaxial air jet

Coaxial air jet systems have been intensively studied for cell encapsulation; these systems employ an air jet around the solution jet to increase the force acting on nascent droplets. This method produces uniform droplets ranging from one millimeter to a few hundred micrometers. However, the system usually requires limited flow rate, less than 30 mL/hour, to avoid formation of a liquid jet. Also, the size distribution broadens when the droplet diameter decreases or solution viscosity increases. Because the system cannot handle viscous solutions, thus-produced microcapsules are usually coated with polycation to reduce the pore size and to provide immunoprotection for the encapsulated cells, but the coating might not be biocompatible [27]. For these reasons, the coaxial systems have not been considered suitable for scale-up.

1.3 Overview

In this study, we fabricated particles of natural hydrogel polymers and studied the feasibility of employing these particles for applications involving controlled drug delivery and tissue engineering.

Described In Chapter 2 is the electric field assisted precision particle fabrication (E-PPF) method that we utilized to fabricate monodisperse gelatin

microspheres (GMS) and to study parameters affecting the drug release from the basic gelatin which is a common carrier for protein, peptide or gene due to its ability to form polyionic complex with opposite-charged biomolecules. Uniformity of the GMS allowed us to study the drug release behavior without uncertainty resulting from wide size distribution. Specifically, we addressed the effects of the cross-linker, glutaraldehyde (GA), on drug release behavior, drug distribution within polymer matrix, polymer degradation, and the matrix ability to form polyionic complex with the drug. This information allowed the development of a mathematical model to predict the release of water soluble agents from cross-linked GMS.

Chapter 3 describes cancer-targeting delivery of chemotherapeutics via surface modified gelatin particles fabricated via the E-PPF method in an effort to increase the efficacy of chemotherapy. Also, an improved feature of the E-PPF apparatus that is particularly suited to fabricate sub-micron sized hydrogel microspheres is outlined.

Chapter 4 outlines a capsule generator utilizing mechanical vibration to break coaxial jets. Also described is a feature designed to sort out empty capsules in the case of cell encapsulation, which is necessary to minimize the volume of the capsules be transplanted. The cross-linking of the alginate capsule was studied by monitoring the penetration of the calcium ion and measuring the intraparticle distribution of alginate.

Conclusions and future work are described in Chapter 5.

CHAPTER 2

DRUG RELEASE PROFILE AND ITS MODELING FOR UNIFORM BASIC GELATIN MICROSPHERES UNDER DIFFERENT CROSS-LINKING DENSITIES

2.1 Introduction

Gelatin has attracted much attention in many biomedical applications because of its excellent biocompatibility and its degradability to non-toxic products [28,29]. The isoelectric point of gelatin derived from collagen can be modified during fabrication [30]. This unique aspect allows one to design and form a polyionic complex between a charged biomolecule and a gelatin of the opposite charge. For these reasons, gelatin is commonly utilized in tissue engineering and gene therapy [31-35]. For example, the release profiles of ^{125}I-labeled basic fibroblast growth factor (bFGF), transforming growth factor-β1 (TGF-β1), bone morphogenetic protein-2 (BMP-2) and vascular endothelial growth factor (VEGF) [33,35] from acidic or basic gelatin in disk or microparticle forms have been studied. Gelatin microparticles were also employed to increase the transfection probability at the delivery site by the controlled release of plasmid DNA *in vivo* [34]. In spite of extensive applications reported, little comprehensive quantitative analysis has been available to date, which could be used for predicting and designing the release profiles of gelatin microparticles as drug carriers.

Mathematical modeling is important to systematically explore and design potentially new devices for controlled release [9]. In general, release of a water soluble active agent from degradable matrix devices is determined by a reciprocal action of the following processes [36]: (a) diffusion of the external aqueous medium into the device, (b) relaxation of the polymer matrix, including swelling, (c) liberation of the immobilized active agent due to hydrolytic or enzymatic degradation of the matrix, (d) diffusion of the mobile active agent from the bulk of the matrix to its surface, and (e) diffusion across the boundary layer. These processes are interrelated, which makes general mathematical modeling a formidable task. Mladenovska et al. assumed a biexponential function for the release from hydrogel devices based on the frequently-observed biphase release pattern for hydrogel [37]. Although the presumed biexponential function does simplify the mathematical formulation, the fundamental mechanisms responsible for the biphasic release pattern have not been elucidated. It is also known that not all the release profiles follow the biphasic pattern [38,39]. As a result, phenomenological models which account for only the release-limiting factors have been developed.

Swelling or hydration has often been considered to predict the release from hydrogel devices. In this case the resulting models depend on the swelling interface number [15], S_w, which is empirically adjusted for the release process [40,41]. Attempts were also made to take into account viscoelastic response and diffusion during polymer swelling [42]. Although some of these models produced results in agreement with experimental data, they required many adjustable

parameters [43]. Recently, a unified mathematical model was proposed to predict drug release from surface and bulk eroding hydrolyzable polymer matrices with all parameters obtained prior to the controlled release experiments [44]. The model, however, was limited to polyester and polyanhydride due to the specific assumption of the polymer degradation kinetics and exclusion of the enzymatic effect in the model. Tzafriri [36] reported a drug release model from polymer matrices entirely or partially due to the enzymatic polymer degradation, but no effects of cross-linker concentrations were included in the model. Therefore, to the best of our knowledge, no mathematical model proposed to date is suitable to predict drug release from gelatin microspheres (GMS) while accounting for the processing parameters.

Herein, we propose a mathematical model to account for the release of a water-soluble active agent from uniform GMS, incorporating polymer degradation and specific drug distribution as a function of the cross-linking agent concentration. Specifically, the current model combines a diffusion-reaction equation, which accounts for the polyionic complexation between the drug and gelatin matrix, with polymer degradation and drug distribution dictated by the cross-linking agent concentration. Basic GMS of 100-μm diameter (wet) were used for the study. The effective diffusivities were determined by fitting Fick's diffusion model to *in vitro* release of trypan blue, an acidic model drug, from GMS in the absence of collagenase. The relationship between the enzymatic degradation rate of GMS and the concentration of glutaraldehyde (GA), a cross-linking agent, was obtained by fitting the proposed model to the *in vitro* release

data from GMS cross-linked with the GA concentrations of 0.125%, 0.375% and 0.875% v/v in phosphate buffered saline solution in the presence of collagenase. The obtained degradation parameter was then used for the present model to predict the release of trypan blue from GMS cross-linked with GA concentrations of 0.25% and 0.625% v/v.

2.2 Materials and methods

2.2.1 Materials

Basic gelatin (IEP=9.0, Mw=100kDa) was provided by Nitta Gelatin Co., Osaka, Japan. Span 85 (Sigma–Aldrich), hexane (Fluka), acetone (Sigma–Aldrich), canola oil (Schnucks), 25% glutaraldehyde (GTA) (Sigma–Aldrich), trypan blue (Sigma–Aldrich) and phosphate buffered saline (PBS) (Sigma-Aldrich) and collagenase 1A (Sigma-Aldrich) were purchased from Sigma-Aldrich, USA. Alexa fluor 430 was purchased from Invitrogen. All materials were used as obtained.

2.2.2 Preparation of microspheres

GMS were prepared using electric field assisted precision particle fabrication method (E-PPF). Briefly, gelatin was dissolved in warm DI water (50-60 ^{o}C) to make a 5% w/v solution which passed through an inner nozzle concentric with an outer nozzle carrying a liquid stream immiscible with the gelatin solution. The setup was applied with mechanical vibration using an

ultrasonic transducer (Branson Ultrasonic) controlled by a function generator (Hewlett Packard, Model 3225A). The disturbance caused the polymer stream to break up into uniform droplets, which were collected in a cold mixture of oil, hexane and span 85 (2-6 ^{o}C) to expedite the gellation process. The gelled GMS were then treated with acetone, centrifuged, and dried in a lyophilizer (Labconco, freezone 4.5 L) for a day.

2.2.3 Cross-linked gelatin microspheres

The GMS were cross-linked with glutaraldehyde (GA) using a method reported by Tabata et al. [45] with some modification. Briefly, the dry spheres were dispersed in a desired concentration of GA solution of pH 5 at 4 ^{o}C for 24 hours, transferred to a glycine solution at room temperature to deactivate the remaining GA [45]. The resulting spheres were then washed with DI water and lyophilized.

2.2.4 Drug impregnation

An aqueous solution containing the drug (0.1% w/v of trypan blue or Alexa fluor) was dropped into a known amount of GMS (5 µl/mg) and left for two hours. The drug solution was completely absorbed into the GMS because the volume of the drug-containing solution was less than the theoretical swelling volume of GMS.

2.2.5 Characterization

GMS were observed under optical microscopy and scanning electron microscope (Hitachi 4700) for morphology and sphericity. Uniformity of GMS was investigated by measuring the size of 50 particles.

Cross-linked GMS were weighted in air-dry conditions and then immersed in phosphate buffer saline (PBS, pH 7.4) at room temperature for 24 hours and their wet weight was measured. The swelling ratio of cross-linked GMS was defined as the weight increase after swelling divided by the weight of dry GMS.

The gelatin solution (5% w/v) was cross-linked under different GA concentrations (0.125, 0.25, 0.375, 0.625, and 0.875 % v/v) at 50 ℃ for 5 hours. The resulting solutions were rapidly cooled to –50 ℃ and lyophilized. The cross-linked gelatin was ground into small particles and then suspended in PBS (pH= 7.4) after filtration (5-μm pore). The zeta-potential of the suspension was measured five times using Malvern Zetasizer 3000.

The intraparticle drug distribution of Alexa Fluor 430, investigated as a function of cross-linker concentrations, was obtained by measuring the fluorescence intensity distribution at the equatorial cross-section of the GMS using a confocal laser scanning microscope (CLSM, Olympus Fluoview FV 300 Laser Scanning Biologic Microscope). The drug distribution was measured, immediately after loading and after 15 days to remove all mobile drug with PBS, to account for the total and the ionically-complexed drug, respectively [46].

The images obtained were converted into intensity plots and radial distributions by averaging the intensity at a given radial distance from the GMS

center. The resulting intensity plots were linearly fitted and normalized so that the drug amount inside the microsphere corresponded to the amount observed in the release experiment. The distribution of mobile drug was assessed by subtracting the distribution of the 'complexed drug' from the initial drug distribution.

2.2.6 *In vitro* drug release

The drug-loaded GMS were incubated in two release media, prepared using phosphate buffered saline (PBS) with and without an enzyme (collagenase 1A, 373 ng/ml), at 37 ℃ for 18 days with continuous agitation. The supernatant was sampled at scheduled time intervals and its optical absorption was measured spectrophotometrically using Gilford Response Spectrometer.

2.3 Theory and mathematical models

2.3.1 Release paradigm and case definition

During the process of loading a finite amount of drug via hydration of the polymer matrix, drug molecules move inwards by diffusion and capillary forces, forming a polyionic complex with gelatin or remaining free inside the microsphere [39]. If the amount of the drug loading is in excess of that, gelatin can immobilize; this loading process results in two pools of drugs encapsulated in the microspheres: 'mobile drug' which is free to diffuse and 'complexed drug' which is immobilized by the gelatin matrix and released only upon matrix degradation. The determinants of the initial distribution of mobile and complexed drug include

the cross-linking agent concentration, the microsphere size, and the isoelectric point of gelatin. In the present model, we incorporated the initial distribution of mobile or complexed drug obtained from the fluorescence intensity distribution of drug at the equatorial cross-section of the GMS. By doing so, we introduced in the model the heterogeneous immobilizing strength of cross-linked GMS.

When dispersing GMS in a buffer solution, water or buffer solution begins to hydrate the matrix and mobile drug starts to diffuse out while complexed drug remains stationary within the microspheres. Hydration in GMS can be assumed not to be a rate-limiting process and to be negligible because it is much faster than the release. The matrix geometry could also be assumed to remain unchanged during the release process because of the fast hydration. This assumption of invariant geometry is likely to hold since gelatin degradation is a bulk degradation process [47]. In addition, it can be assumed that the surface of the microspheres is most resistant to erosion and that the sphere remains the same size until most of the drug has been released, which is valid for most cross-linked gelatin where the cross-linker is introduced from outside via absorption [46].

With the gelatin degradation catalyzed by collagenase, both mobile and complexed drug are released. The degradation depends on both the cross-linking density of gelatin and the enzyme activity. A single diffusion coefficient was used in the model with which we implicitly assumed that the degradation-liberated drug behaved similarly to the mobile drug and that the heterogeneous cross-linking density within the GMS introduces negligible changes in diffusivity

throughout the microsphere. This was justified by the fact that the diffusivity increased only 1.5 times in our experiment when the cross-linking agent concentration increased sevenfold. The diffusion coefficient was also hypothesized to be time-invariant during the particle degradation. This assumption is valid if most of the drugs are released prior to disintegration of GMS or significant matrix degradation leading to nearly invariant polymer density.

2.3.2 Model development

The release of the drug is assumed to be governed by a diffusion-reaction equation with a source term due to the liberation of the complexed drug initially immobilized in polymer matrix via the polyionic attraction between the drug and the polymer. Consider a spherical shell at a radial distance r where the concentration of the diffusing substance is C and the mobile substance generating in the element is C_s as shown in Figure 2.1. Assume the diffusion is isotropic along the radius, and the equation describing the release can be obtained:

$$\frac{\partial C}{\partial t} = \frac{1}{r^2}\left\{\frac{\partial}{\partial r}(Dr^2\frac{\partial C}{\partial r})\right\} + \frac{\partial C_s}{\partial t} \tag{2.1}$$

where D is the diffusion coefficient of the drug through the polymer matrix. The equation is solved using the following boundary conditions:

$$\left.\frac{\partial C}{\partial r}\right|_{r=0} = 0 \tag{2.2}$$

$$C\big|_{r=R} = 0 \tag{2.3}$$

where R is the radius of the GMS. The boundary condition, Equation (2.3), arises from the assumption of an infinite sink: that is, the rate at which the drug diffuses to the surface of the microsphere equals the rate at which the drug leaves the microsphere. Hence there is no accumulation of the drug on the surface [48].

The diffusion constants could be obtained by modeling the first three-day release profiles from GMS in PBS solution without enzymatic degradation of polymer matrix. In this case, the second term on the right-hand side of Equation (2.1) becomes zero. The initial condition for this case is

$$C(r)\big|_{t=0} = C_{m0}(r) \tag{2.4}$$

where $[C_{m0}(r)]$ is the initial distribution of the mobile drug. This drug distribution within GMS was obtained as described in section 2.4.

In drug release accompanying polymer degradation, the liberation rate of the complexed drug in the gelatin spheres participating in the diffusion process is associated with enzymatic polymer degradation mechanism. In general, enzymatically-catalyzed polymer degradation can be described by the Michaelis-

Menten equation [36,49,50] as shown in Equations (2.5)-(2.7) where K_M represents the Michaelis-Menten constant, k kinetic parameter, E enzyme, S polymer and P final product. Usually $V_{\max}$ and K_M are constants for a given enzyme-substrate pair.

$$E + S \underset{k_{-1}}{\overset{k_1}{\rightleftharpoons}} ES \xrightarrow{k_2} E + P \tag{2.5}$$

$$\frac{\partial [S]}{\partial t} = -k_2 [E]_0 \frac{[S]}{K_M + [S]} = -\frac{V_{\max} [S]}{K_M + [S]} \tag{2.6}$$

$$K_M = \frac{k_{-1} + k_2}{k_1} \tag{2.7}$$

It has been known that collagenase is efficient in catalyzing hydrolysis of collagen with k_2/K_M up to 10^6 $M^{-1}S^{-1}$ [51], when the most efficient enzyme is defined with k_2/K_M in a range of 10^8-10^{10} $M^{-1}S^{-1}$ (perfect enzyme) [52]. Since gelatin is more susceptible to degradation than collagen, we assume that collagenase catalyzes a reaction each time the enzyme molecule encounters gelatin molecule and that an upper theoretical limit has thus been reached for the efficiency, which suggests the limit $[S] \ll K_M$ and also very little ES complex is formed, thus $[E]_0 \approx [E]$. By applying this limit to Equation (2.6), it reduces to

$$\frac{\partial [S]}{\partial t} = -\mu [S], \quad \mu = V_{\max} / K_M \tag{2.8}$$

Equation (2.8) suggests that the degradation rate of the polymer matrix is a function of polymer concentration characterized by parameter μ which should be a function of GA concentration and enzyme concentration but independent of time if the total enzyme concentration does not change over time. In this *in vitro* experiment, the collagenase concentration was fixed to 373 ng/ml, which mimics the synovial fluid of a patient with osteoarthritis.

Seeing that immobilization of drug molecules in GMS is ascribable to the polyionic attraction between them, the liberation rate of immobilized drug is assumed to be proportional to the polymer degradation rate or equivalently, the immobilizing capacity of polymer substrate σ is a constant, i.e., $C_i = \sigma S$, where C_i denotes the concentration of complexed drug; thus, the liberation rate of complexed drug can be derived from Equation (2.8):

$$C_i(t) = C_{i0} e^{-\mu t} \tag{2.9}$$

where C_{i0} is the initial distribution of complexed drug.

Note that the relationship between C_i and the concentration of liberalized drug C_s is $C_s = C_{i0} - C_i$ and, therefore,

$$\frac{\partial C_s}{\partial t} = \mu C_{i0} e^{-\mu t} \tag{2.10}$$

Substituting Equation (2.10) into Equation (2.1), the diffusion equation for small molecule release from a gelatin microsphere degraded by enzyme becomes

$$\frac{\partial C}{\partial t} = \frac{1}{r^2}\left\{\frac{\partial}{\partial r}(Dr^2\frac{\partial C}{\partial r})\right\} + \mu C_{i0}e^{-\mu t} \tag{2.11}$$

This model accounts for the drug release mediated by both the initially mobile drug and the drug liberated during the polymer-degradation process. The nonuniform distributions of initially mobile drug and complexed drug are also included in this model via the initial conditions, Equation (2.4) and Equation (2.10).

The relationship between the degradation-related release constant μ and GA concentration is now required for the release to be determined by Equation (2.11) with no adjustable parameters. To achieve this, firstly, the parameter μ was chosen to minimize the sum of squares of the differences between the experimental release data and the solution of Equation (2.11) for GMS cross-linked with three GA concentrations: 0.125%, 0.375% and 0.875% v/v. Subsequently, a numerical equation relating μ and the GA concentration could be established.

2.4 Results and discussion

Figure 2.2 shows the scanning electron micrographs of the dry GMS before and after cross-linking. It is evident that the cross-linked GMS lost their

spherical shape when they were dehydrated because of the pores/voids in the matrix, but regained spherical shape after water-uptake as seen in Figure 2.2(C). The average size of the swollen GMS is 100 μm. Because the actual drug release took place in an aqueous media, it was important to retain the uniformity of the swollen GMS to be able to predict the release profiles of the active agents without the uncertainties associated with the GMS size.

The swelling ratio of GMS was measured to evaluate the cross-linking extent of GMS as shown in Figure 2.3. The swelling ratio reduces as the GA concentration increases from 0.125 to 0.25% v/v, but fluctuates after 0.25% v/v. The diminution in swelling ratio is likely due to the increase in the density of the polymer matrix after cross-linking and the decrease in the free volume for the water molecules to penetrate into [53], while the fluctuation might be ascribed to higher cross-linking at the surface of GMS limiting the further reduction of swelling ratio. The heterogeneous cross-linking within the GMS probably resulted from the large GMS size used in this study causing significant concentration gradient of GA in the GMS along the diffusion path. It is unlikely that GA concentration above 0.25% v/v reacted with all the amino groups in the GMS because zeta potential of cross-linked gelatin showed continuous decreases as the GA concentration increased, as shown in Figure 2.4. Zeta potential is the potential difference between the dispersion medium and the stationary layer of fluid attached to the dispersed particles. In other words, it is a measure of the overall charge a particle acquires in a specific medium. Thus, the change in the charge of gelatin molecules due to cross-linking density could be identified by

measuring the zeta potential of homogeneously cross-linked gelatin particles. The fall in zeta potential also suggests less attraction between cross-linked basic gelatin and the opposite-charged drugs. The fluctuation of swelling ratio might also be attributed to hydrophilicity of the cross-linker. The hydrophilicity of the gelatin matrix increases as the degree of cross-linking via the GA, a hydrophilic compound, increases resulting in a favorable condition for the hydration of GMS. With the GA concentrations used in this study, hydrophilicity and density of gelatin compensated for each other, giving rise to similar diffusive release profiles [54].

To obtain initial conditions for the proposed model and to elucidate the release behavior of the cross-linked GMS as a function of GA concentration, the drug distribution in the GMS as a function of GA concentration was investigated. Figure 2.5(A) shows the total drug distribution including both mobile drug and complexed drug within the GMS, indicating that the initial drug concentration was higher at the center for the sample with 0.125% GA but slightly lower for the ones with 0.375 and 0.875% GA. This could be attributed to the suppressed drug diffusion resulting from the smaller and/or fewer pores of the highly cross-linked GMS [46].

Figure 2.5(B) shows the distributions of the complexed drug which were normalized to its percent amount obtained from the release profiles, exhibiting a higher concentration at the center of the GMS in all cases. The combination of the nonunform distribution of complexed drug within GMS which is higher at the surface and lower near the center and the lower attraction between acidic drug

and gelatin with the increase of GA as shown in Figure 2.4 suggest an inhomogeneous cross-linking with GMS. The extent of inhomogeneous cross-linking would become more significant at a higher GA concentration because of the fact that cross-linking starts from the surface, impeding the inward diffusion of GA.

The initial mobile drug distribution was obtained by subtracting the distribution of complexed drug from that of the total drug. The distribution of mobile drug was determined by the drug loading mechanisms and the polyionic attraction between the drug and the polymer during the drug loading process. The release of the mobile drug from the GMS was most likely through simple diffusion and contributed to the initial burst in the release profile. Therefore, initial burst might be reduced by lowering the amount of drug that is diffusively loaded into the GMS.

The diffusion constants were obtained by solving the diffusion equation with the initial mobile drug distribution in a manner to model the first three-day drug release profiles by pure diffusion, as described in section 2.3.2. The diffusion constants were chosen to minimize the R-squared value. The comparison between the experimental data and thus-obtained results predicted by the model and the corresponding diffusion constants are shown in Figure 2.6(A) and (B). A fitting curve using a power function with an R-squared value of 0.99 is also shown in Figure 2.6(B) which can be used to predict diffusion constants from GMS cross-linked with different GA concentrations. Although constants for the fitting curve might vary as different drugs are employed

because of drug mobility, the trend is likely to remain the same due to the cross-linking density of gelatin, producing a good estimation in the case of different drugs. The diffusion constants are seen to generally decrease with increasing GA concentrations. This may be due to higher diffusion barrier resulting from denser polymer matrices and reduced free volume accessible by the penetrating water molecules because cross-linking agents shorten the polymer chains between the cross-links. It is seen in Figure 2.6(A), however, that the drug release rates from GMS first fall in the absence of matrix degradation, then rebound when cross-linking agent concentration exceeds 0.375% v/v. These results may imply that, without taking into consideration of other effects, the diffusion constants obtained would not be a monotone function of cross-linking agent concentration, which was explained in [55] as an inaccuracy resulting from using a single diffusion model. However, our work suggests that by incorporating accurate drug distribution, diffusivity of a diffusion model depends reciprocally on GA concentration, proving the importance of the drug distribution inside the GMS to correctly account for the drug release behavior.

The degradation-related release constant μ as a function of GA concentration that was needed to complete the mathematical model was derived by using it as a fitting parameter in Equation (2.11) to calculate the drug release from the GMS cross-linked with GA concentrations of 0.125%, 0.375% and 0.875% v/v while minimizing the sum of squares of deviations from the experimental release data with the diffusivities used as before. Figure 2.7 shows the model prediction and experimental results. To include the effect of cross-

linking agent concentration in the model, an empirical exponential decay function fit was used to relate the degradation constant to GA concentration, as shown by Equation (2.12).

$$\mu = 0.36(1 + 0.1\exp^{(-14.29 \times C_{GA})}) \tag{2.12}$$

where C_{GA} is the volume percent concentration of GA used to cross-link GMS. This dependence was specifically chosen as it gave the best fit to the data (R^2> 0.99). The slower decrease of μ as GA concentration rises agrees with the saturating effect of GA concentration on impeding the release. This phenomenon may be elucidated by the cross-linking process facilitated by diffusion and the stronger diffusion barrier resulting from higher GA concentration, as described earlier. According to the Michaelis-Menten equation (Eqs.(5)-(7)), the degradation constant μ is proportional to the enzyme concentration or its square due to anomalous diffusive motion of the enzyme when the gelatin matrix is large [56]. Therefore, Equation (2.12) could be modified to make it applicable to other enzyme concentrations without further experiments.

With the degradation-related release constant μ predicted by Equation (2.12), the diffusion-reaction equation, Equation (2.11), was solved to predict the release from the GMS treated with 0.25% and 0.625% v/v GA. The comparison between model predictions and experimental data is shown in Figure 2.8. A good agreement is seen between the model and the experimental data, which may be attributed to the fact that the model accounts for the non-uniform drug distribution,

the drug-binding ability of the polymer matrix and the polymer degradation rate, which are all influenced by the cross-linking agent concentration. The reasons for the slight difference between the model prediction and experimental data may be as follows: as mentioned earlier, the diffusivities used in the model were assumed to be constant within the microsphere throughout the release process. It is reasonable, however, to anticipate some variations of diffusion coefficient within the microsphere and during the drug release process as the polymer matrix degradation progresses. Also, the degradation-related constant μ and diffusion constant *D* were assumed to be independent of the locations inside the GMS whereas the cross-link density is a function of radius. In this model, the effect of heterogeneous cross-linking density was considered to affect only the ability of the gelatin matrix to bind with the drug and, therefore, the resulting drug distribution within the microsphere. However, since the predictions of the present model are in reasonable agreement with the experimental data, it may be concluded that the radial variation and time-dependence of the degradation-related constant and diffusion coefficient resulting from heterogeneous cross-linking and degradation rate are not significant.

2.5 Summary

Monodisperse GMS were fabricated and cross-linked with GA by the E-PPF method to investigate the effects of GA concentration. It was shown that the swelling ratio of GMS decreased as the GA concentration increased, but leveled off at higher GA concentrations. The stabilization might be attributed to

inhomogeneous cross-linking within the microspheres because of the large size of the GMS used in this study or the competing effects such as hydrophilicity and cross-linking ability of GA. The zeta potential measurements suggested that the higher GA concentration led to lower drug-gelatin complexation. The intraparticle distribution patterns of total drug, the addition of mobile and complexed drug, indicated that more drug molecules accumulated near the GMS surface as the GA concentration increased, probably due to higher diffusion barrier. The nonuniform distribution of complexed drug suggested inhomogeneous cross-linking within GMS which is more evident as GA concentration increases. At higher GA concentrations, the GMS surface would be more cross-linked, resulting in more resistance to degradation and less gelatin-drug complexation.

A mathematical model based on drug diffusion and enzymatic degradation (Michaelis-Menten kinetics) of polymer matrix as a function of cross-linking agent concentration was proposed to describe the release of an acidic drug from cross-linked basic GMS. The model takes into consideration the initial intraparticle distribution of the mobile and complexed drug affected by GA concentrations. Diffusion constants are inversely dependent on the GA concentration in spite of the fact that the release rate is not a monotone decreasing function of GA concentration. A relationship, Equation (2.12), between the degradation-related release constant and the GA concentration was obtained which, when incorporated into the model, produced results in good agreement with the experimental data with no adjustable parameters. It is, therefore, concluded that

the present model may serve as a useful tool in predicting drug release from GMS.

2.6 Figures

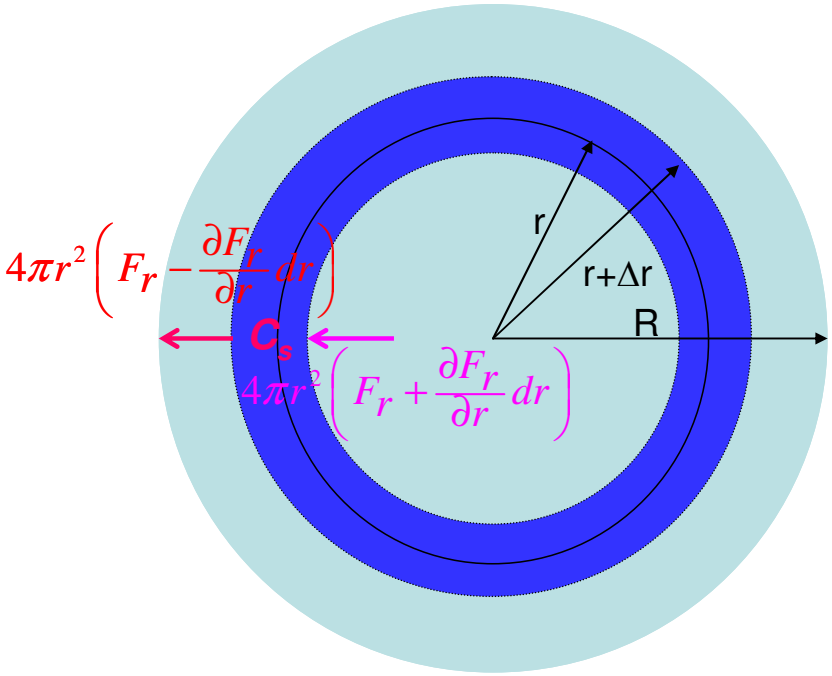

Figure 2.1 Scheme of drug release from a gelatin microsphere.

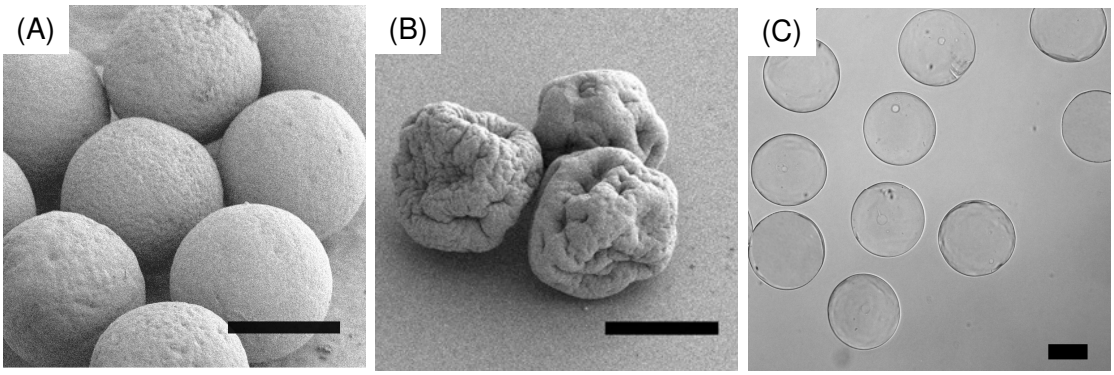

Figure 2.2 Gelatin microspheres observed in dry state under SEM before cross-linking (A), after cross-linking (B) and in wet state under OM (C). The scale bars are 30 μm, 30 μm and 50 μm for (A), (B) and (C), respectively.

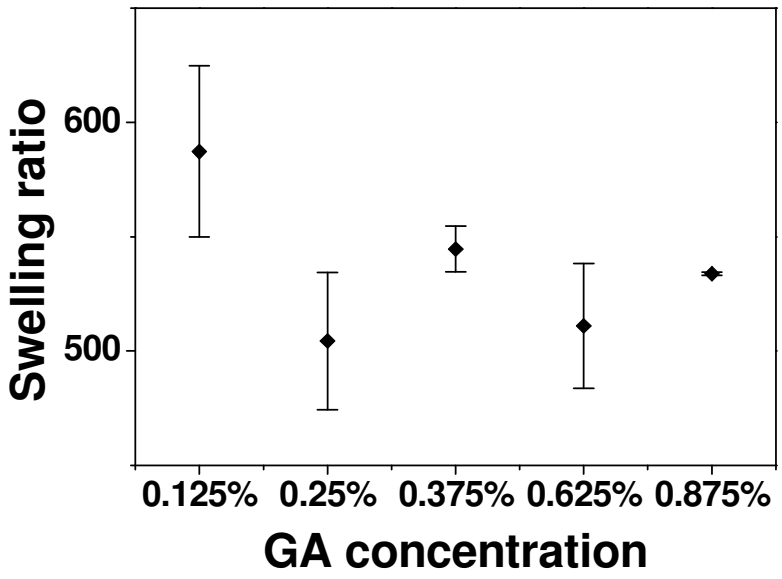

Figure 2.3 Swelling ratios of gelatin microspheres as a function of glutaraldehyde concentration.

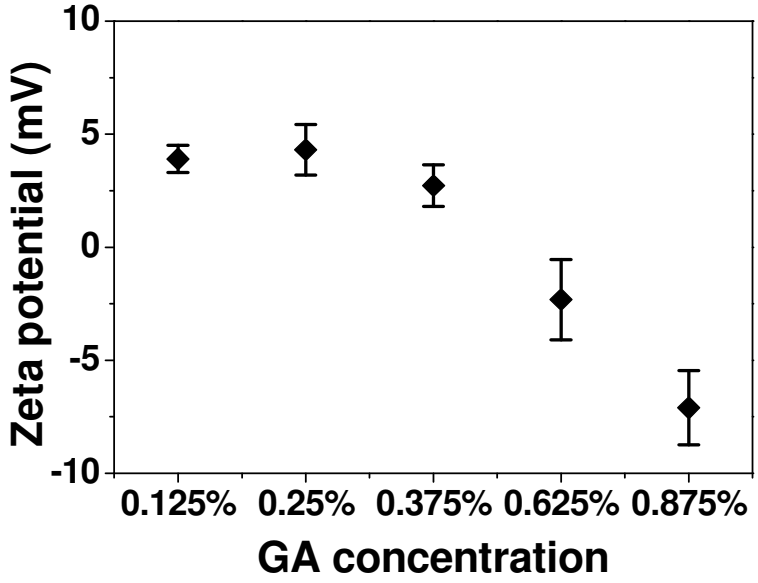

Figure 2.4 Zeta potentials of cross-linked gelatin as a function of glutaraldehyde concentration.

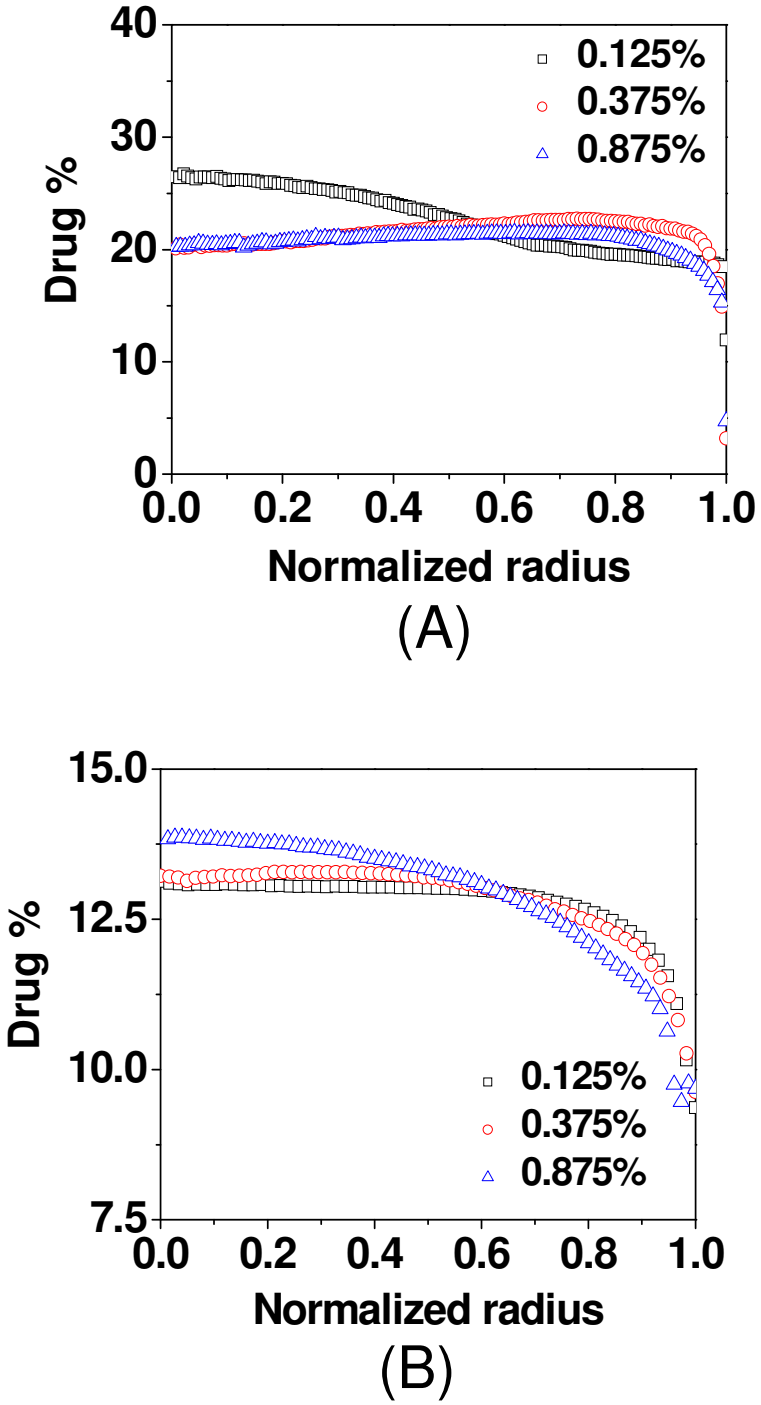

Figure 2.5 Initial distributions of total drug (A) and complexed drug (B) within the gelatin microspheres cross-linked with glutaraldehyde.

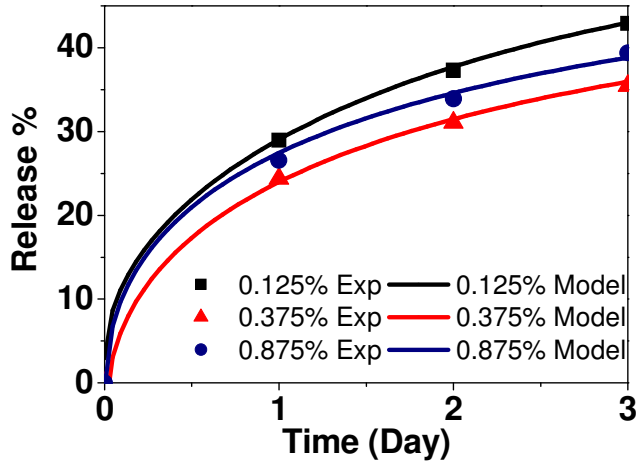

(A)

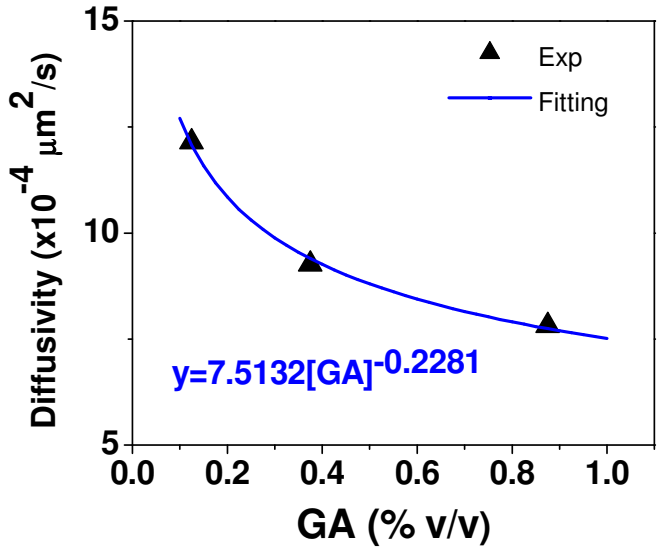

(B)

Figure 2.6 *In vitro* drug release from the gelatin microspheres as a function of glutaraldehyde concentration and their respective model results in the absence of enzyme (A) and the corresponding diffusivities obtained via the model (B).

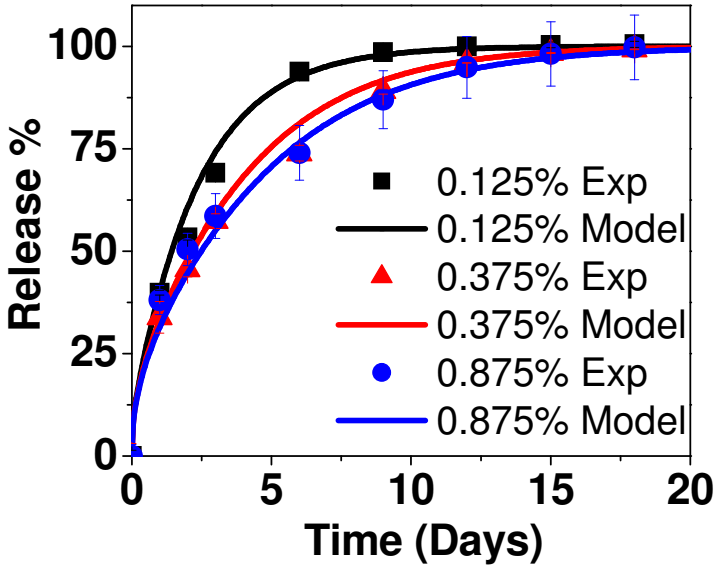

Figure 2.7 Model and the experimental results of *in vitro* drug release from the gelatin microspheres cross-linked with glutaraldehyde in the presence of enzyme with degradation parameter 1, 0.38 and 0.36, respectively.

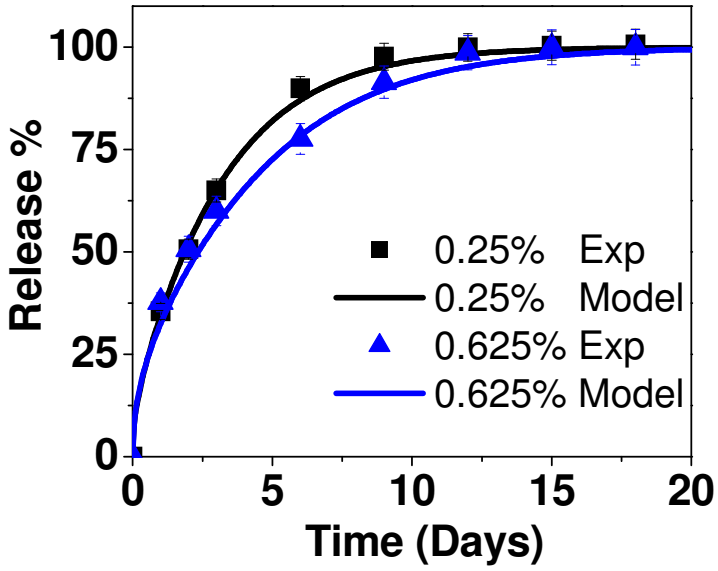

Figure 2.8 Model predictions and *in vitro* drug release from the gelatin microspheres cross-linked with glutaraldehyde in the presence of enzyme.

CHAPTER 3

GELATIN PARTICLES AS A DRUG CARRIER SYSTEM FOR CANCER TARGETING

3.1 Introduction

Cancer is a class of diseases in which a group of cells multiply beyond the normal limits, invade adjacent tissue (invasion) and sometimes spread to other locations in the body via the lymphatic or blood system (metastasis). In 2007, the American Cancer Society reported 7.6 million cancer deaths globally. Chemotherapy is one of the most effective cancer treatment methods by impairing cell division, effectively targeting fast-dividing cells; however, off-target cancer drug uptaken by benign tissues often causes systemic damage and serious side effects. For example, doxorubicin (DXR), one of the most effective and widely used anticancer drugs, causes acute adverse effects including nausea, vomiting, anorexia and heart damage (cardiotoxicity) [8,9,57] which considerably limit the effectiveness of DXR and other chemotherapeutics. Therefore the prevention of untargeted therapeutic drug release in the blood circulation system is the key to improve outcomes of modern chemotherapy.

Several strategies have been proposed to target cancer cells, mostly based on biodegradable polymeric particles because of their stability [6], versatility of surface modification [7] and potential for different drug release characteristics [8-10]. Particle drug carriers were reported to be concentrated preferentially near tumor sites ascribable to the enhanced permeability and retention (EPR) effect of fast-growing tumor vasculature, mitigating off-target

drug delivery [58-60]. Though accumulation rate of particles at tumor sites increased with particle drug carrier, off-target drug release still existed because of the rapid drug release of nanoparticles during circulation. Therefore, potent cancer targeting drug carriers should be triggered to release drug only when they are at expected tumor sites.

Particles with surface modification have also been reported for cancer targeting based on the recent discovery of over-expression of many molecules in cancer patients, including CA125 and human kallikrein 10 for ovarian cancer [61,62], prostate-specific antigen (PSA) and cysteine-rich secretory protein-3 for prostate cancer [63,64], cytokine colony-stimulating factor-1 (CSF-1) for endometrial carcinoma [65], protein 7B2 for medullary carcinoma of the thyroid [66], chromogranin A for endocrine and neuroendocrine tumors [67], Cathepsin D for breast tumors [68] and many more. One cancer targeting strategy utilizes particles conjugated with antibodies that recognize tumor-associated antigens; this strategy has shown promising *in vivo* results as potential diagnostic or prognostic of tumors [69]. The *in vivo* application, however, might be restricted on account of weak linkage stability and potential immunogenicity after repeated injections [70]. Particles conjugated with proteins to facilitate the recognition of tumor-specific antigens as vaccine [71] might suffer from similar obstacles *in vivo*. Due to these limitations, these methods might not be promising in treating cancer. A better strategy for cancer targeting drug delivery might be the design of a peptide recognizing these over-expressed molecules in cancer sites; this strategy has shown promising *in vivo* results as a potential diagnostic or prognostic of

tumors [72] combined with drug release that is triggered only at expected tumor sites.

In this work, we describe surface-modified GMS as a vehicle for the targeted delivery of DXR to treat breast malignancy. The drug carrier consists of GMS core fabricated via the electric field assisted precision particle fabrication (E-PPF) method using an acidic gelatin, loaded with DXR [46,73] and a high-density peptide layer whose hydrolysis is catalyzed by Cathepsin D, a specific protease secreted by the breast cancer cells. Thus, the core is protected from general proteolysis, wherein DXR is safely contained, until the peptide shell is removed through Cathepsin D-assisted hydrolysis prominent in the proximity of breast cancer cells. As the peptide shield is removed, gelatin is exposed to general proteases, triggering the release of DXR. As a result, the drug is released only in the vicinity of the target cancer cells and its release rate is controlled by the protease concentrations. This way, the most effective chemotherapy may be achieved with minimal side effects. The E-PPF method was modified to reduce the size of GMS fabricated.

3.2 Materials and methods

3.2.1 Materials

The starting materials were gelatin type B from porcine skin (225 bloom, Sigma–Aldrich,), span 85 (Sigma–Aldrich), hexane (Fluka), acetone (Sigma–Aldrich), canola oil (Schnucks), 25% glutaraldehyde (GTA) (Sigma–Aldrich), sodium hydroxide (Fluka), toluidine blue O (Sigma–Aldrich), 1-ethyl-3-[3-

dimethylaminopropyl] carbodiimide hydrochloride (EDC), N-hydroxysuccinimide (NHS) and doxorubicin (DXR) (Sigma–Aldrich), phosphate buffered saline (PBS) (Sigma-Aldrich) and dimethyl sulfoxide (DMSO) (Fisher).

3.2.2 Preparation and cross-linking of microspheres

Gelatin microspheres (GMS) were prepared using the E-PPF method described in section 2.2.2. GMS of sub-micron sizes were fabricated through a modified E-PPF method in which the electric field applied was increased to induce the amount of charge leading to spray of smaller droplets which was monitored using video camera. Sample collection was performed as described in section 2.2.2.

The GMS were cross-linked with glutaraldehyde (GA) described in section 2.2.3 with pH of the solution adjusted to 9 using 0.2M sodium hydroxide. To evaluate the effects of the polymer matrix density and the drug-immobilizing ability, different GA concentrations were used for cross-linking.

3.2.3 Peptide conjugation

500 µL of 0.1 M PBS solution, 100 µL of 0.33 M EDC, and 100 µL of 0.5 mM NHS solution were mixed to form PBS-EDC-NHS solution as catalysts for the conjugation [74]. To this mixture, 200 µL of 100 nM peptide which consists of a Phe-Phe-Arg-Asp sequence, a Mca fluorophore molecule ((7-methoxycoumarin-4-yl)acetyl) at the C-terminus, and a darker quencher molecule

(dinitrophenyl, abbreviated as Dnp) near the N-terminus (synthesized by BioMol) and drug-loaded GMS were added and stirred overnight. The resulting mixture was centrifuged and washed with DMSO to collect peptide-conjugated GMS.

3.2.4 Drug impregnation

Cross-linked GMS were impregnated with a model drug, TBO or DXR, by adding an aqueous solution in a ratio of 5 µl/mg GMS and cured for 24 hrs at room temperature. Loading efficiency of TBO as a function of pH of drug medium and cross-linking of GMS was determined by measuring absorbance of TBO with spectrometer (Gary-5G) at wavelength of 630 nm.

3.2.5 Characterization

Morphology and uniformity of GMS were examined through SEM (Hitachi 4700) after platinum coating. Zeta potentials of the cross-linked gelatin were determined using dynamic light scattering technique (NICOMP 380 ZLS Particle Sizer), and swelling ratios of GMS cross-linked with different GA concentrations were measured as described in section 2.2.5.

3.2.6 *In vitro* drug release profiles

The *in vitro* release study of DXR from the drug-loaded GMS with and without the peptide surface coating was performed in the presence of Cathepsin D enzyme, MCF7 culture media, 3T3 culture media or Hela culture media. Drug release was assessed by directly sampling the supernatant and measuring the

fluorescence emission from DXR molecules which is measured using the microplate reader (excitation of 470 nm and emission of 585 nm). Protease-, DNA-, and RNA-free water (Fisher Scientific) was used for the measurement.

3.2.7 *In vitro* chemotherapy on cancer cells

MCF7 (ATCC), 3T3, and Hela cells were cultured in petri dishes and let grow till nearly confluent. Drug-loaded GMS conjugated with peptides were added into the cell cultures media. Optical images were taken every two hours for 10 hours. Trypsin-EDTA (ATCC) was used to trypsinize the cells for viable cell counting. Cell counting was done using hemocytometer (Neubauer) with trypan blue stain (Sigma-Aldrich) for cell viability tests.

3.3 Results and discussion

The SEM and optical images in Figure 3.1(A) and (B), respectively, illustrate that the GMS fabricated via the E-PPF method are spherical and uniform in size: 30 ± 2 (dry) and 65 (wet) μm in diameter. The confocal laser scanning microscopy image in Figure 3.1(C) shows the distribution of the impregnated DXR in the GMS, measured at 580 nm. DXR (pKa=8.2) is expected to interact electrostatically with the gelatin matrix, whose IEP was measured to be 5 as shown in Figure 3.2(A).

The DXR molecules immobilized by the gelatin would be delivered to the targeted cancer site without being released while the unbound ‘free’ molecules

are released systemically via diffusion. Therefore, maximization of the drug bound to the GMS matrix, i.e. the drug loading efficiency, is crucial in the mitigation of the off-target release. To study the factors affecting the loading efficiency, TBO was chosen as a model drug with a pKa value of 7.9, close to that of DXR, 8.2, and impregnated into the GMS cross-linked with 0.625 % v/v GA. Figure 3.2 (B) shows the loading efficiency measured as a function of pH of the impregnation medium, exhibiting that the efficiency was improved generally as the pH increased. In a basic environment, the negative charge of the gelatin would be enhanced by the deprotonation of its carboxyl groups, which was supported by the zeta potential decrease with pH (Figure 3.2(A)). On the other hand, the protonation of TBO would be promoted in the acidic media of pH lower than the pKa of the drug [27]. Therefore, the increase in the loading efficiency observed in the basic media indicated that the former effect was more dominant than the latter on promoting the electrostatic interactions between the gelatin and TBO.

The effect of GMS cross-linking on the drug loading efficiency was investigated using the GA concentrations of 0.125 – 0.875% v/v. Figure 3.3(A) shows that the loading efficiency increased with GA concentration until it reached 0.625% but decreased afterwards. The acidity of gelatin would increase with GA concentration, i.e., cross-linking, due to the consumption of its amino groups in the cross-linking process. This was confirmed by the zeta potential of the gelatin measured as a function of GA concentration (Figure 3.3(B)), leading to the increase in the loading efficiency. However, at a GA concentration of 0.875%, the

loading efficiency was observed to decrease, indicating that the acidity was not the only factor affecting the efficiency. With the cross-linking, the density of the gelatin matrix increases, which would cause more hindrance for inward diffusion of the drug during the loading process due to the decreased water content of the GMS. Figure 3.3(C) shows the decreased swelling ratio, i.e., the water content, of the GMS as a function of GA concentration. The matrix density may not be a dominant factor affecting the drug diffusion when it is low, but becomes significant when high, off-setting the electrostatic effect. This could account for the decreased loading efficiency observed for the GMS cross-linked with 0.875% GA.

Drug release profiles of DXR from GMS with and without peptide coating incubated in pure buffer solution, purified Cathepsin D solution, purified collagenase 1A solution, secretion with culture media of MCF7 human breast cancer cells, 3T3 mouse fibroblast cells and Hela cells were expressed as fluorescence intensity of DXR (Figure 3.4) which is assumed to be proportional to drug concentration. More drug is released from GMS than from peptide coated GMS when incubated with and without collagenase, which is a common protease in the body facilitating hydrolysis of gelatin. This observation suggests that the peptide coating layer hinders the diffusive release and degradation of gelatin. The drug release from GMS with peptide coating is prohibited in most of the above cases except for the purified Cathepsin D solution and MCF7 breast cancer cell secretion proving the targeting function of the peptide coating layer. The drug release difference between these two cases might be explained by the

different concentrations of Cathepsin D secreted by MCF7 cells and the purified Cathepsin D or other proteases secreted by MCF7 cells. For instance, it has been known that MCF7 cells also secrete into culture media collagenase [75] assisting the hydrolysis of GMS, which likely contributes to the increased release of DXR compared to the case of Cathepsin D. The slight fluorescence increase in the case of 3T3 cells might also be attributed to similar secretion of collagenase by 3T3 [76]. The enhancement of drug release ascribable to collagenase-assisted hydrolysis of gelatin leading to the dissociation of the drug carriers was also observed in Figure 3.4 showing increasing fluorescence intensity from both coated and uncoated GMS cultured with collagenase 1A. Drug release from the coated GMS, however, is still much suppressed compared to the nude GMS with or without the presence of collagenase 1A. This evidence once again proved that the peptide layer on the drug carrier particle surface dramatically diminishes the non-specific drug release.

Figure 3.5 shows the number of viable cells for three cancer cell lines at every two hours after the addition of the peptide coated GMS loaded with DXR. As shown in Figure 3.5, the number of both 3T3 fibroblast and Hela cells increases because of the cell proliferation, indicating negligible cytotoxicity to these two non-targeted cells secreting no aspartic protease (e.g. Cathepsin D). The lower proliferation rate of 3T3 viable cells after 6 hours might be attributed to the mild DXR release as a consequence of collagenase secreted by 3T3 cells. On the contrary, the number of MCF7 breast cancer cells dropped dramatically to 13% in 10 hours. This result proves that the peptide coating enables the high

specificity of the particle drug delivery system to targeted cancer biomarkers and associated tumor cells.

Figures 3.4 and 3.5 were obtained by Dr. Munima Haque under the supervision of Professor Logan Liu who collaborated with us on this work.

The concept of utilization of peptide-coated GMS as a drug carrier targeting breast malignancy has been demonstrated to be effective *in vitro*. For particles to be injected intravenously, they should be smaller than the diameter of capillaries, 10 μm, to avoid infarction [77]. Such a size limit might be less stringent for gelatin particles because of their elasticity. The E-PPF method utilizes vibration waves on a liquid jet to produce uniform droplets (Figure 3.6(A)) and employs the electric field so that droplets are charged and Coulomb repulsion between droplets prevents recombination (Figure 3.6(B)). The droplet size is mainly restricted by the jet diameter and thus-produced GMS are usually larger than 50 μm (wet). With the increase of electric field came the increase of induced charge on droplets and the breakup of droplets because the Coulomb repulsion force overcame the surface tension and viscosity of the solution [78] as seen in Figure 3.6(C). This method utilized generation of uniform microdroplets to avoid the formation of Taylor cone before spraying, which was difficult because of high conductivity of the water as the solvent. Figure 3.7 shows the SEM image of gelatin particles of 50 μm in diameter produced with an applied voltage of 5 kV, demonstrating the modified E-PPF method could be employed to fabricate particles suitable for intravenous injection.

3.4 Summary

Peptide-coated GMS are developed as a cancer targeting drug carrier. Release of drug complexed to the gelatin matrix is triggered by the biomarker protease enzyme Cathepsin D secreted by breast cancer cells and their extracellular matrix. Drug loading efficiency was optimized by controlling the cross-linker concentration and pH of drug solution. With the peptide-coated GMS, the specificity of cancer chemotherapeutic drug delivery is expected to be improved significantly and the adverse side-effects are to be reduced due to the mitigated off-target drug release. The E-PPF method could be modified to produce GMS much smaller than the jet diameter, suitable for *in vivo* application, via the applied electric field.

3.5 Figures

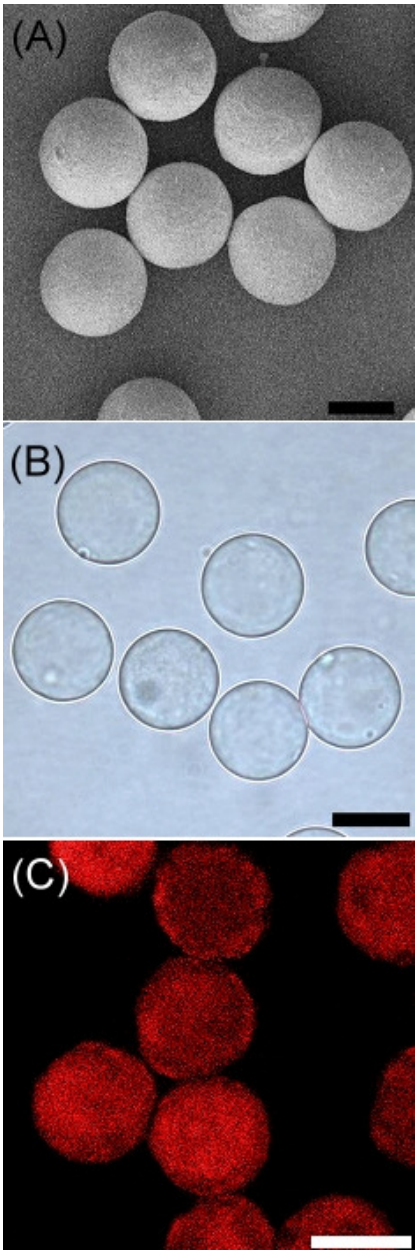

Figure 3.1 Gelatin microspheres observed in dry state under SEM before cross-linking (A), after cross-linking in wet state under OM (B) and after doxorubicin loading under CLSM (C). Scale bars are 20, 50, and 50 μm for (A), (B), and (C), respectively.

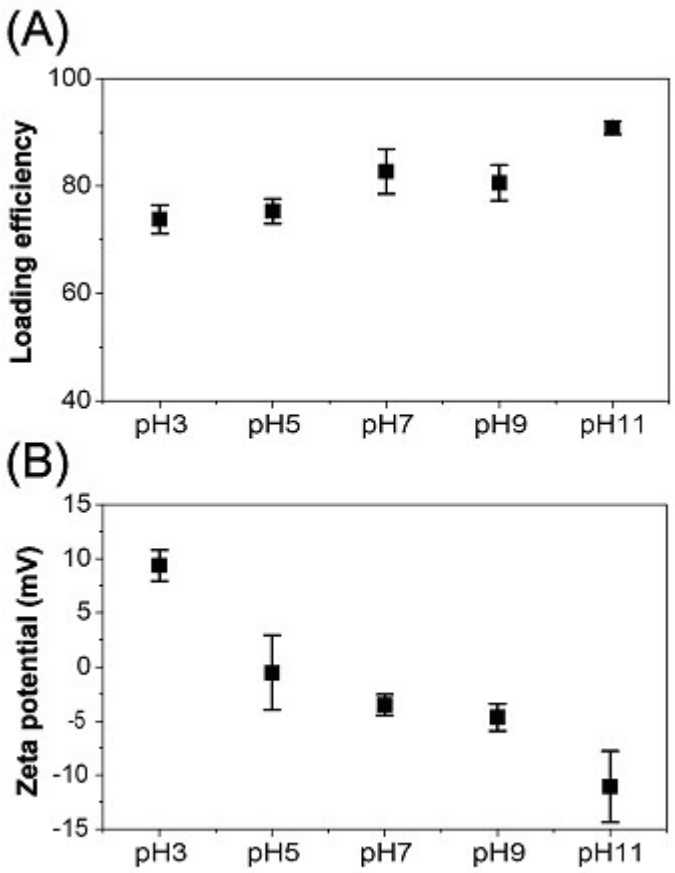

Figure 3.2 Drug loading efficiencies in gelatin microspheres (A) and zeta potentials of gelatin as a function of pH (B).

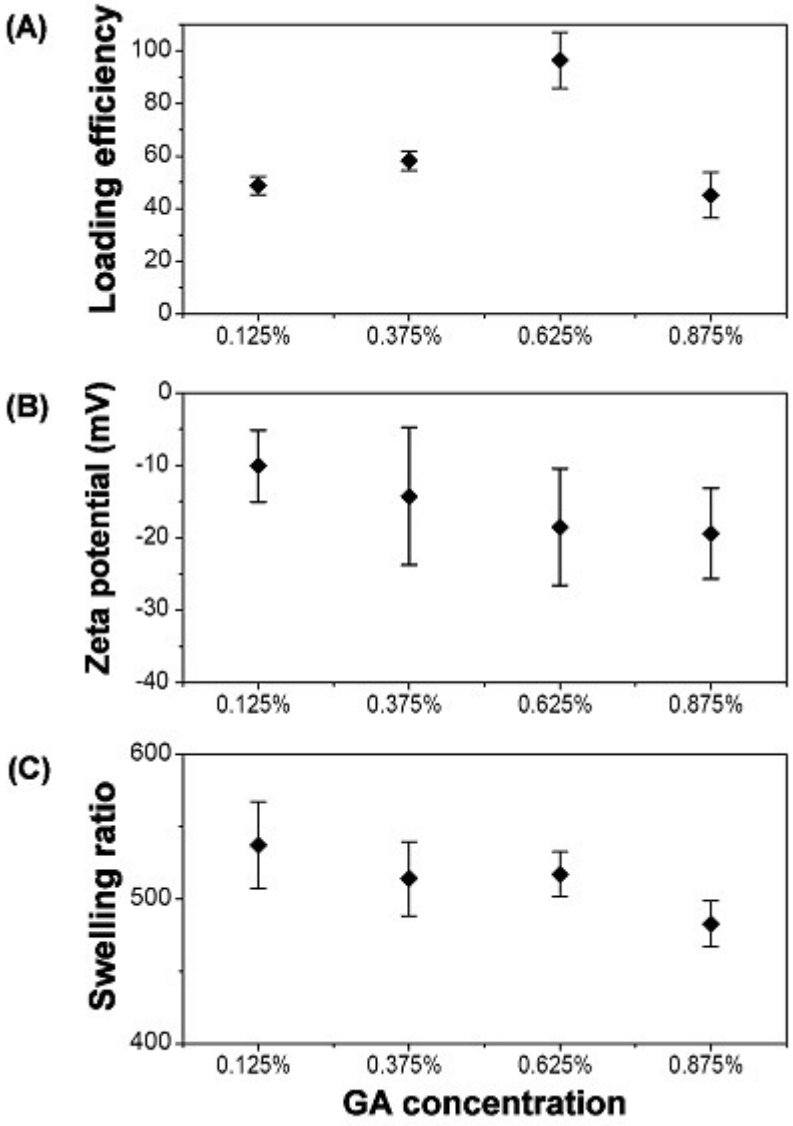

Figure 3.3 Drug loading efficiencies (A), zeta potentials (B) and swelling ratios as a function of glutaraldehyde concentration.

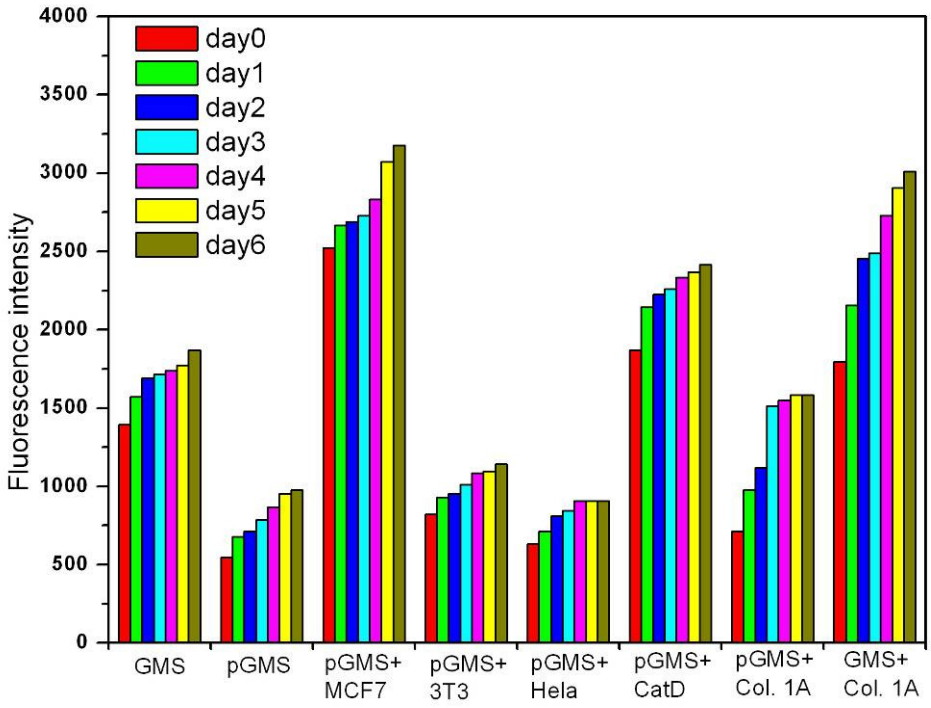

Figure 3.4 Fluorescence intensity of released drug from the gelatin microspheres in various incubation conditions. Abbreviations used in the figures: pGMS for peptide coated gelatin microspheres; CatD, Cathepsin D; Col. 1A, collagenase 1A.

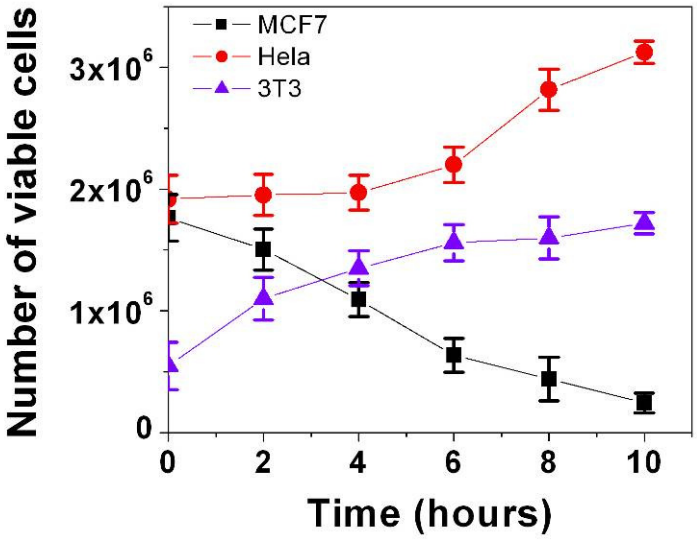

Figure 3.5 Viability of MCF7 human breast cancer, human Hela and 3T3 mouse fibroblast cells after exposure to the peptide-coated gelatin microspheres loaded with doxorubicin.

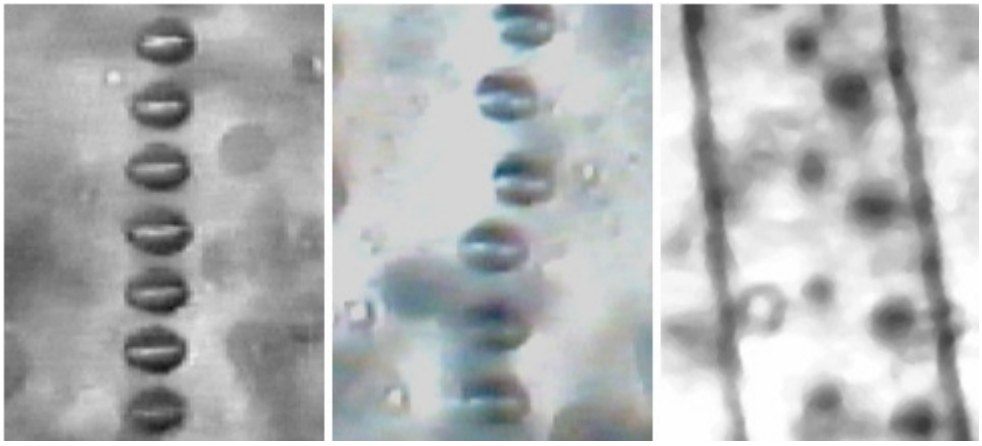

(A) (B) (C)

Figure 3.6 Gelatin droplets of 100 µm generated via E-PPF method with applied electric potentials of 0 V (A), 200 V (B) and 2.5 kV (C).

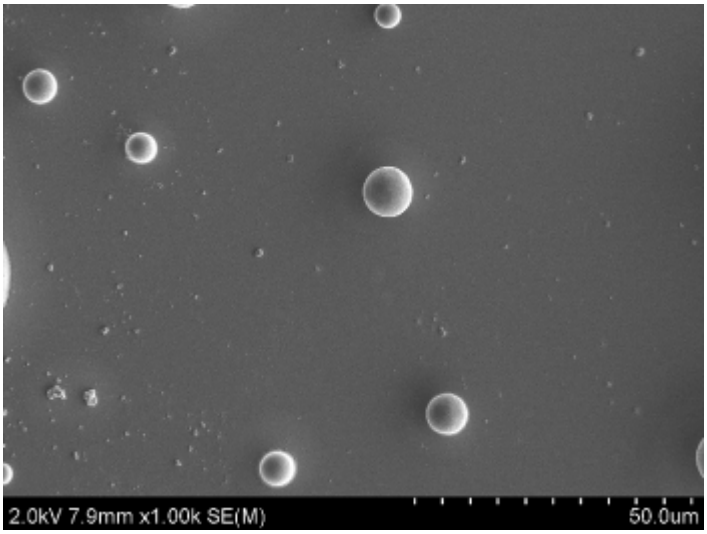

Figure 3.7 SEM image of dry gelatin particles.

CHAPTER 4

FABRICATION, CHARACTERIZATION AND SORTING OF ALGINATE MICROSPHERES/MICROCAPSULES FOR CELL ENCAPSULATION

4.1 Introduction

Encapsulation of living cells in a semi-permeable system has been developed over the past decades as a strategy for tissue and organ replacement and long-term controlled release of therapeutic agents. In 1980, Lim et al. reported the first successful implantation of microencapsulated islet of Langerhans which led to numerous efforts at achieving xenotransplantation without immunosupression [79]. Later, encapsulation of hepatocyte cells was investigated as a supportive device, either to allow liver regeneration upon acute liver failure or extend liver function until a transplant is available [14,80]. In addition to primary cells, encapsulation of genetically engineered cells secreting therapeutic proteins has also been proposed to target various diseases and malignancies while delivery of genes producing proteins via transcription and translation has not demonstrated definitive clinical value at present [81]. Table 4.1 shows an overview of some encapsulated cells for protein delivery [81].

In 1997, Wang et al. thoroughly screened polymers for cell encapsulation based on cytotoxicity and cell attachment properties [82]. Among the materials tested, alginate showed the lowest cytotoxicity and best cell attachment. Other materials such as poly(ethylene glycol) (PEG) [83], hyaluronic acid [84,85], chitosan [86], agarose [87], and synthetic polymers have also been tested for cell encapsulation. However, alginate has been and still is the most important

biomaterial for cell encapsulation. Alginates are natural polysaccharides extracted from seaweed consisting of homopolymeric regions of β-D-mannuronic acid (M-blocks) and α-L-guluronic acid (G–blocks) and interspersed with regions of MG blocks. The constituents of alginate affect greatly the properties for the purpose of cell encapsulation [88-95]. The ratio and arrangement of mannuronic acid and guluronic acid affect the dimension stability and gel strength greatly because of their different binding efficiency to divalent ions such as Ca^{2+}, Ba^{2+}, and Sr^{2+}, which are the most common cross-linking agents for alginate [94]. Also, studies indicate a high content of M-blocks in alginate (more than 85%) can provoke undesired immune reactions [96,97].

Cell encapsulation using alginate microcapsules is usually performed by dispersing the alginate solution drops containing cells into an aqueous solution containing cross-linking agents. The whole process is carried out in aqueous solution which is favorable to keep cells alive. Various methods have been developed to produce drops including dripping [91], coaxial air jet [98], electrostatic dripping [99], mechanical cutting [100] and jet break-up [101]. Despite remarkable progress in the cell encapsulation technology, several obstacles still need to be overcome for viable clinical applications. The main considerations for the encapsulation technology include the following: (1) uniform microcapsules of controlled sizes for different applications, (2) high production rates to minimize processing time and therefore stress to cells, (3) no air bubbles trapped inside microcapsules which might limit diffusion and weaken long-term gel stability [102], (4) handling of high viscosity alginate solutions to ensure

immunoisolation and (5) low number of void microcapsules, namely, high efficiency of cell encapsulation.

To fulfill such requirements, the precision particle fabrication (PPF) method was adopted and modified for cell encapsulation, which was developed to fabricate uniform microspheres and microcapsules of poly(lactide-coglycolide), ethylcellulose, chitosan and other polymers. In this chapter, a novel cell encapsulation technology for fabricating alginate microspheres/microcapsules of precisely controlled sizes of 150-600 μm in diameter is described. Properties of thus-fabricated alginate microspheres/microcapsules and viability of encapsulated cells were examined. The feasibility of sorting void capsules from the ones containing cells was demonstrated by employing a detection and electric deflection system.

4.2 Materials and methods

4.2.1 Materials

Sodium alginate used in this study was purchased from Sigma-Aldrich (intrinsic viscosity of 250 cp, 2% (25^{o}C)) or obtained from laminaria hyperborean (SF120, FMC Biopolymer, Drammen, Norway). Mannitol (VWR), calcium chloride (Fluka), barium chloride (Aldrich), sodium chloride (Fluka), blue dextran (Sigma), murexide (Fluka) and rhodamine B (Sigma) were purchased.

4.2.2 Preparation of alginate microspheres and cell encapsulation

Sodium alginate (2-3.5% w/v) was dissolved in purified water and filtered through 0.22 µm-pore filter paper for sterilization. Sodium chloride (0.15M) or mannitol (0.3M) was co-dissolved in the alginate solution to maintain osmotic pressures of human pancreatic islet cells. In some cases, mouse fibroblast cells or bovine liver tissues were dispersed in alginate solution for encapsulation. The protocol for encapsulation of human pancreatic islet cells was adopted from the work of Norwegian University of Science and Technology [103].

A coaxial dual-nozzle was used to produce a cell-containing jet surrounded by polymer solution which is disrupted into uniform droplets by a piezoelectric transducer controlled by a frequency generator. The droplets generated in the air were observed via video camera and recorder to determine the droplet size and collected in an aqueous gelling solution ($CaCl_2$ or $BaCl_2$) with stirring. The spheres were left in the gelling solution for less than 5 minutes to minimize stress to cells. The distance between the nozzle and the collection bath was optimized to produce uniform alginate microspheres while other fabrication parameters were fixed. The diameter of the outer nozzle opening and the vibration frequency were also varied to fabricate microspheres/microcapsules of different sizes. The resulting microspheres were filtered with mesh and washed several times with purified water or culture media. For some cases, oil or a blue dextran solution was fed through the inner nozzle during the fabrication of alginate microcapsules to observe the material passing through the inner nozzle.

4.2.3 Characterization

More than 150 microspheres fabricated under different conditions were examined and visualized by optical microscopy to determine the size and uniformity of each sample. The distribution of alginate molecules within the microsphere was examined by staining them with Rhodamine B. Alginate microspheres fabricated were dispersed in 0.5% w/v Rhodamine B solution and washed with DI water after 3 hours to remove the excess dye molecules. Rhodamine B bound to alginate was observed via a confocal laser scanning microscope (CLSM, Olympus Fluoview FV 300 Laser Scanning Biologic Microscope).

The penetration of the cross-linking agent, calcium ion, through alginate was examined using murexide as a complexometric indicator. A drop of alginate solution with 100 μM murexide was placed into a Petri dish containing calcium chloride solution, resulting in an alginate sphere with a diameter about 3 mm while the whole process was observed under optical microscope. Three different concentrations of sodium alginate and calcium chloride solutions were used for this study: [Alginate]: 2, 3 and 4% w/v, and [$CaCl_2$]: 50, 100 and 200 mM. The hardened alginate spheres were observed under optical microscope and images were taken at designed time intervals.

4.2.4 Cell viability

Viability of pancreatic islet cells before and after encapsulation was assessed according to a dual fluorescent staining technique, fluorescein

diacetate (FDA)/ propidium iodide (PI) [104]. FDA, a nonfluorescent derivative of fluorescein, can penetrate the cell membrane and be deacetylated by nonspecific esterase resulting in accumulation of fluorescein within cells as a sign of viability when only the nuclei of membrane-compromised cells will be bound by PI fluorescing red, a sign of cell death. Stock solution of FDA (5 mg/ml in acetone) and PI (20 µg/ml in Dulbecco's phosphate buffered saline (DPBS)) were stored in the dark at 4 ^{o}C. Staining was performed with FDA which was freshly prepared by adding the stock solution to 10 ml of DPBS to a final concentration of 20 µg/ml and PI stock solution. Pancreatic islet cells before and after encapsulation were washed with Hank's balanced salt solution (HBSS) and re-suspended in 1 ml of HBSS before staining. Cells were stained by adding 0.1 ml of FDA working solution and 0.03 ml of PI stock solution and examined under a fluorescence microscope (Olympus IX81) 3 minutes after the addition of the dyes. The ratio of cell number to dye was approximately 2×10^{6} cells to 2 µg of FDA plus 0.6 µg of PI.

4.2.5 Sorting scheme

Sorting of void and cell-containing microcapsules can increase cell encapsulation efficiency by eliminating void ones. Sorting of cells and chromosomes has been achieved via electrostatic deflection of charged droplets, similar to the method used for ink-jet printers [105]. Despite the advances in this technology, the popularity of this sorting technique is limited due to the expensive detection method involving laser sources which might also cause damage to cells.

In this study, optical microscopic imaging and digital image processing were employed to detect cells in the microcapsules generated from the encapsulator.

Figure 4.1 shows the illustrative scheme of the sorting function equipped in the encapsulator. The encapsulator generates uniform droplets to place the point at which droplets break off from the main stream (breakoff point) at a fixed distance downstream from the observation point. During the time a cell traverses the observation point and reaches the breakoff point (drop delay), the measurement result is sent to the sort logic control and then the decision signal is sent to the droplet charging circuit. Charge can be applied to droplets via direct charging or indirectly by putting a charging ring at the breakoff point. The droplet stream containing charged or uncharged droplets passes through the electric field between the two metal plates to which high voltages of opposite polarities have been applied. Sorting can be achieved by deflecting the charged droplets out of the main stream.

To estimate the transverse distance a charged droplet traveled, average induced charge on droplets was measured using a Fluke 87V multimeter. The droplets were caught in a metallic plate connected to a grounded 10 MΩ resistor, and the electric current passing the resistor could be measured. The theoretical value of induced charge on the droplet is derived as follows. Assuming the grounded jet is surrounded by a cylindrical electrode with electric potential V_r and radius R_c, the grounded liquid jet of radius r_j can be approximated by solving the Laplace equation (neglecting boundary effect due to finite length of the cylinder) and expressed as

$$E_r = \frac{1}{r}\frac{V_r}{\ln(\frac{R_c}{r_j})} \tag{4.1}$$

where r is the distance from the center of the metal ring on this plane. For simplicity, it is assumed that such electric field surrounds the jet of the wavelength λ, which forms one droplet. By applying Gauss's law, we can derive the induced charge on each droplet as

$$q = \frac{-2\pi\varepsilon_0 V_r \lambda}{\ln(\frac{R_c}{r_j})} \tag{4.2}$$

The wavelength λ, solution velocity and frequency are related by the following equation:

$$v = f \bullet \lambda \tag{4.3}$$

Substituting Equation (4.3) into Equation (4.2),

$$q = \frac{-2\pi\varepsilon_0 V_r v}{f \bullet \ln(\frac{R_c}{r_j})} \tag{4.4}$$

Droplets are slower relative to the jet velocity because of surface tension pulling the liquid back toward the nozzle. The theoretical values of induced charge calculated with jet and droplet velocity were compared with the experimental data.

The electric field intensity E is regarded as uniform distribution in the region between two parallel plates if fringing effect is neglected. The intensity can be expressed as the voltage difference on the two plates, $2V_e$, divided by the distance between them, D. The horizontal acceleration of a droplet with charge q due to the electric field E can be expressed as

$$a = \frac{qE}{m} = \frac{2qV_e}{mD} \tag{4.5}$$

where m is the mass of a droplet. With the acceleration and traveling time, the horizontal distance one charge droplet travels away from the stream could be estimated as Equation (4.6).

$$S = \frac{1}{2}at^2 = \frac{qV_e}{mD}t^2 \tag{4.6}$$

Cell detection is achieved optically with image processing technology without laser or fluorescent dye introduced. Two sorting logic schemes were discussed in this section. The first method is traditional detection based on the fact that encapsulated particles or cells hinder the light from shinning through the

transparent drops or microspheres, causing lower light intensity at the location where the cells or particles locate (light intensity method). An intensity threshold might be tuned to indicate the presence of cells if light intensity was found to be lower than the threshold. The second detection method was based on the fact that the presence of particles would cause sharp intensity variation at the edge of cells or particles (edge detection method). Large light intensity gradient occurs at the periphery of the cell aggregates or in the interface of the alginate solution and air. If we define the location where the gradient is greater than a gradient threshold (GT) as an edge pixel, the presence of cells would increase the number of edge pixels, which can be used to identify the encapsulation of cells. In this study, the GT was empirically determined using the alginate microcapsule containing an ethyl cellulose particle as a model which would be used in determination of cell encapsulation in alginate microcapsules. Optical images of more than 50 alginate microcapsules were examined with the two proposed methods to determine the detection accuracy.

4.3 Results and discussion

Alginate capsules were fabricated by feeding an alginate solution to the nozzle forming a smooth jet which was later broken into uniform alginate droplets via vibration waves during the fabrication. Due to the fast solidification reaction of the alginate, the distance between the nozzle and the collection bath containing the cross-linking agent, the collecting distance, is a crucial parameter for the capsule fabrication. Figure 4.2 shows optical microscopic images of the alginate

spheres collected at three different collecting distances of 3.5, 5 and 10 cm as shown in Figure 4.2 (A-C) ([alginate]: 2 % w/v and [$CaCl_2$]: 50 mM) demonstrating the effect of the collecting distance on the geometry or uniformity of the final product. Figure 4.2 (D) shows the possible fluid conditions based on the morphology of alginate samples. The phenomenon might be explained as follows. The applied vibration destabilizes the stream, making it break into droplets at a critical point (the break-off point) where the mechanical wave applied overcomes surface tension and viscosity. If the collecting distance is shorter than the distance between the nozzle and the break-off point, which is affected by jet velocity, frequency of vibration, viscosity and surface tension of the solution, then no distinct alginate microspheres are collected (Figure 4.2(A)). Once detached from the jet, uniform droplets form resulting in uniform alginate spheres after cross-linking (Figure 4.2(B)). The velocity of droplets is slower relative to the jet velocity when separated from the jet, as surface tension and viscosity of the solution pull the fluid back to the nozzle. Also thin filaments between the droplets might occur for a viscoelastic solution, resulting in different velocities for neighboring droplets. These phenomena could cause droplet coalescence and non-uniform alginate beads (Figure 4.2(C)).

By varying jet diameter and vibration frequency, alginate microspheres of different sizes (150-600 μm) were fabricated. Flow rates were adjusted to form a laminar jet to prevent undesired disturbances from breaking the jet. Laminar jet can be characterized by a small Reynolds number, usually bellow 2300 [105,106], as shown in Equation (4.7) where ρ is the density of the fluid (kg/m^3), Q

volumetric flow rate (m^3/s), η dynamic viscosity (poise) and D_d the jet diameter (m).

$$\mathrm{Re} = \frac{4\rho Q}{\pi \eta D_d} \tag{4.7}$$

Figure 4.3 shows the size distribution of the microcapsules of various mean sizes. Conditions for controlling the capsule size are favorable since the size requirement for encapsulating different cells varies [19,107]. For example, Dufrane et al. showed that pig islets in alginate microcapsules with a diameter of 635 μm survived up to six months after transplantation without immunosuppression [18]. On the other hand, hepatocyte cells in alginate microcapsules larger than 400 μm might not remain viable due to the limited diffusion of oxygen and nutrients [19]. Figure 4.3(B) shows the relationship between the droplet and microcapsule sizes ([alginate]: 2.4% w/v and [CaCl2]: 50 mM). During the solidification process, the significant size shrinkage from droplets to microspheres suggests that dense packing of the alginate molecule chains occurs, which agrees with the theory that alginate solidification is not a point cross-linking but rather a junction-zone. A recent X-ray diffraction study indicated that the junction zone in calcium alginate gel might be described by 3/1 or 2/1 helical conformation (also known as egg-box model) [95,108].

Cross-linking of alginate is required to provide mechanical stability and immunoprotection for cell encapsulation, but the cross-linking process might be adverse to cell viability. Therefore, the processing time should be minimized. To

determine the processing time for sufficient cross-linking of alginate, mureixde, a metal ion chelator, was used to visualize the diffusion of the calcium ion during the gelation process. The color of the murexide molecules changed from purple to light-orange when the chelation with calcium ions in the alginate drops occurred. The boundary between these two distinct colors was observed by optical microscopy (Figure 4.4(A)) to obtain the rates of the calcium ions diffusing into the drops of 2, 3 and 4% w/v alginate solution in 50, 100 and 200 mM $CaCl_2$ bath (Figure 4.4(B)). The diffusion of calcium ions was hindered as the alginate concentration increased because of the increased diffusion barrier and was facilitated as the concentration of the calcium ion increased.

Figure 4.5 shows the non-uniform distribution of the alginate molecules in the microsphere prepared using a 2% w/v alginate solution and a 50 mM $CaCl_2$ bath, suggesting that the gelation process involves not only the motion of the calcium ions but also that of the alginate molecules. Rhodamine B, a cationic fluorescent dye forming a polyionic complex with alginate, provided an approximate distribution of alginate within the microspheres. The migration of alginate is likely due to the attractive force between the alginate and calcium ions since, initially, the polymer distributed uniformly within the droplet.

To visualize the material in the inner tube, canola oil or blue dextran in water was fed into the inner tube to be encapsulated in alginate spheres. Oil encapsulated in the core of the alginate capsule was spherical (Figure 4.6(A)) owing to the interfacial tension between oil and water. Without the interface tension, the blue dextran solution encapsulated in the capsule core was not

spherical (Figure 4.6(B)). However, the blue dextran core enclosed in the alginate microcapsules suggested that the alginate capsules produced via this method would prevent cells from protrusion.

Microencapsulation of various cells has been studied for different therapeutic applications [109]. Mouse fibroblast, bovine liver cells and human islet cells were encapsulated in alginate microcapsules via the present method to demonstrate the feasibility of encapsulating diverse cells (Figure 4.7). Cell viability assay with FDA/PI showed no significant difference in viability (85%) before and after the encapsulation, which suggested the encapsulation did not imperil cells.

The feasibility of cell sorting during encapsulation could be accomplished via electric deflection. To determine the distance droplets traveled during deflection, the induced charge on droplets (pF) was measured and compared with theoretical prediction calculated by Equation (4.4) as shown in Figure 4.8. The theoretical prediction is 1.47 times higher than the experimental result if the velocity of the jet is used in the calculation, while the prediction with droplet velocity is close to the experimental result. The discrepancy between the jet and droplet velocity arises from surface tension and velocity of the solution as described before. With the induced charge on droplets, the distance droplets traveled can be estimated based on Equation (4.6).

The core of the cell sorting system would be the detection of cell-containing and void capsules. Figure 4.9 shows the optical images of alginate capsules used for testing the accuracy of the detection methods. The detection

was achieved via the edge detection method, which was compared with the traditional light intensity method. Figure 4.10 shows the detection accuracy of the light intensity method as a function of light intensity threshold in which cells are assumed to be detected when there is light with intensity below the preset intensity threshold. The accuracy of the detection of cell-containing microcapsules increases as the intensity threshold increases while that of void microcapsules decreases. Intensity threshold of 0.2 gives optimal accuracy of 70% and 95% for detecting encapsulated and empty capsules.

The edge detection method for cell detection requires a reference of gradient threshold and was obtained prior to the experiment using alginate microcapsules containing ethyl cellulose particles as a model. The optical images and the location of edge pixels with the corresponding gradient threshold were shown in Figure 4.11, indicating that the number of edge pixels increases as GT decreases. In the edge detection method, we defined presence of a cell to be when the number of edge pixels was greater than a specific threshold value because edge pixels could be introduced by the periphery of the alginate microdroplet. By presetting the GT as 0.4 and proper edge pixel number 1800, detection accuracies for cell-containing and void capsules were 100% and 95%, respectively, more accurate than the light contract method. Note that the choice of GT for edge pixel number depends greatly on the resolution of the optical image and the size of alginate microcapsules. The edge detection is superior because the intensity of the light source might not affect the results since only the gradient of light intensity has been taken into account for the detection.

4.4 Summary

Uniformly sized alginate microspheres/microcapsules with diameters of 150-600 μm were fabricated for encapsulating cells using the modified PPF method. Non-uniform distribution of the alginate molecules within the microspheres, denser at the bead periphery, and significant size shrinkage from alginate microdroplets to microspheres suggested polymer rearrangements occur during the gelling process, supporting the junction-zone model for the alginate cross-linking process. Cell viability assay of human pancreatic islet cells with FDA/PI shows similar viability before and after alginate encapsulation, which suggests that this technology is suitable for cell encapsulation. A sorting scheme which consists of optical detection method and electric deflection can be annexed to the encapsulator to increase the encapsulation efficiency. The edge detection method is found to be 15% more accurate in cell detection than the light intensity threshold method.

4.5 Figures and table

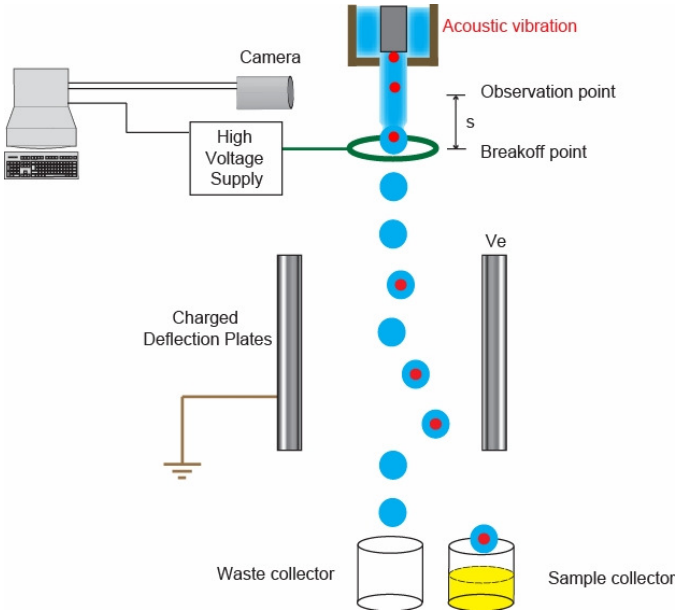

Figure 4.1 A scheme of encapsulator and sorting apparatus.

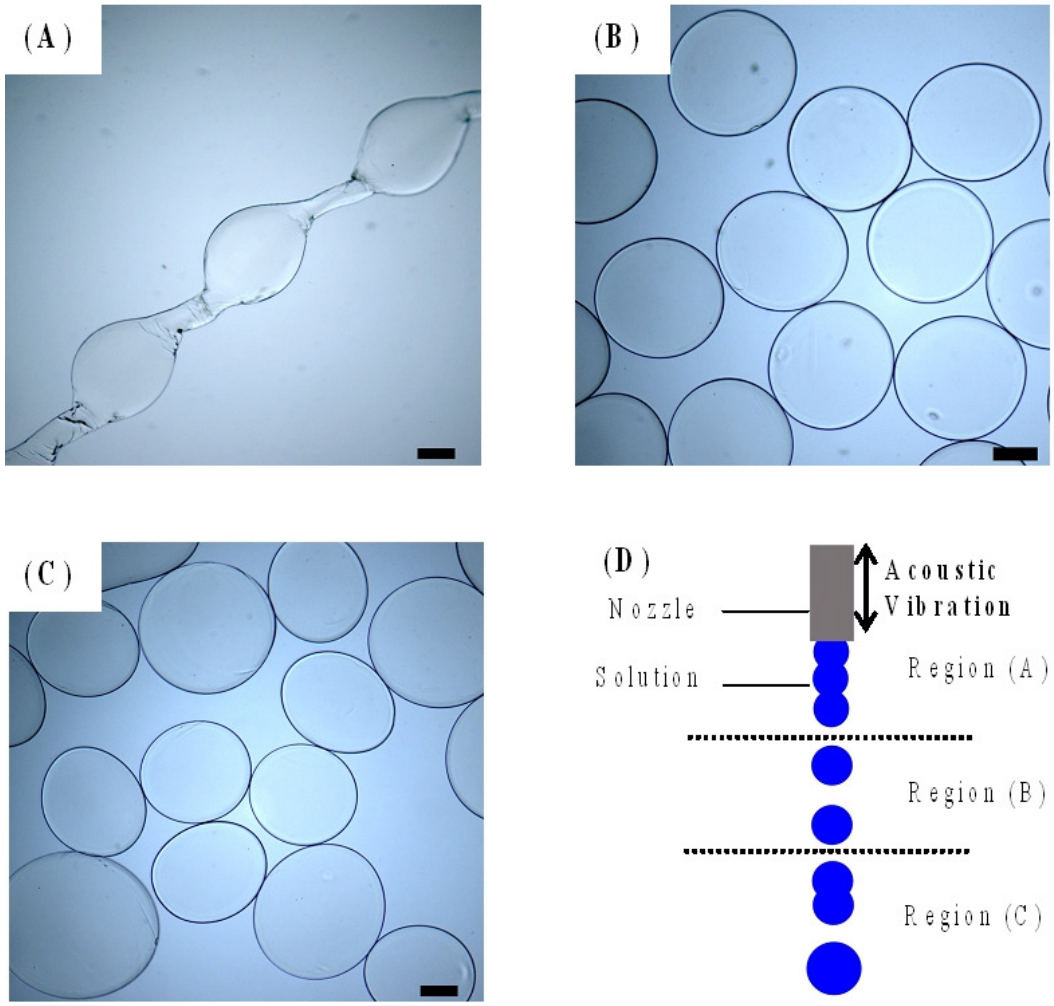

Figure 4.2 Optical microscopic images of alginate samples collected at collecting region of (A), (B) and (C). The scale bars are 200 μm.

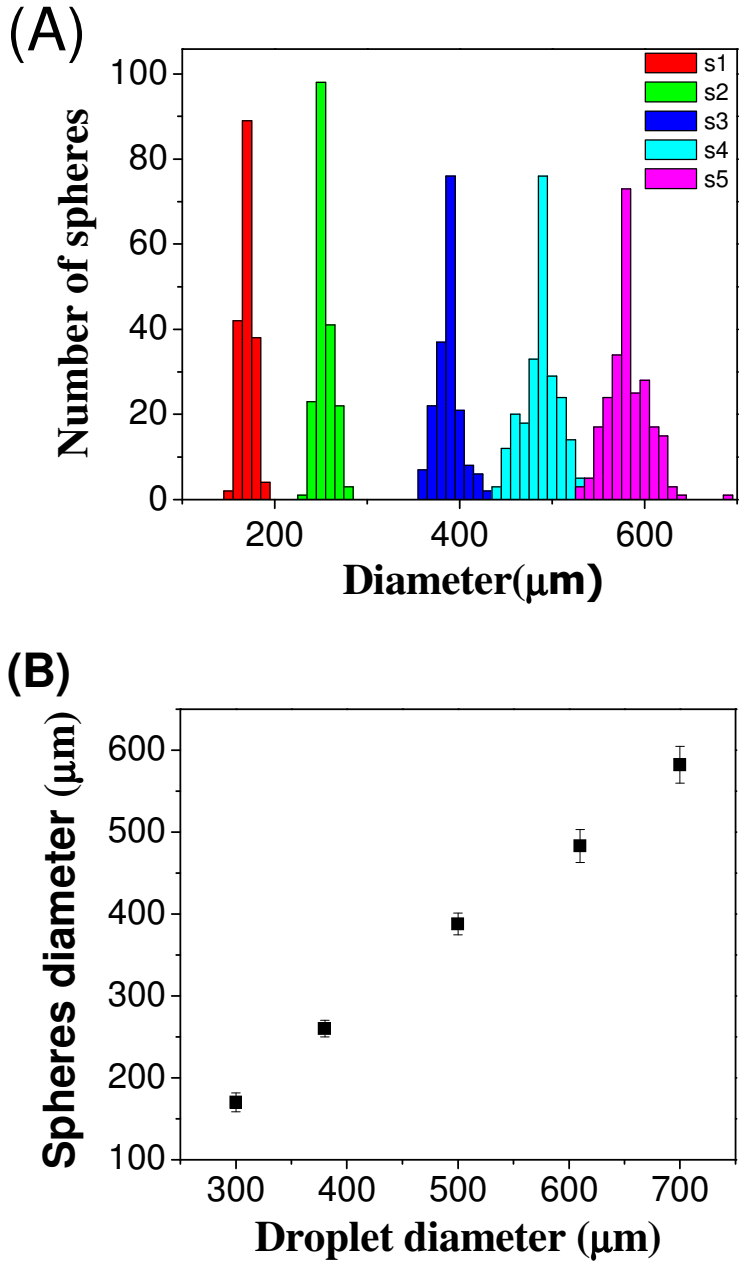

Figure 4.3 Size distributions of alginate microspheres of different sizes (A) and the droplet size vs. sphere sizes from a 2% alginate solution gelled in a 50mM calcium chloride solution (B).

(A)

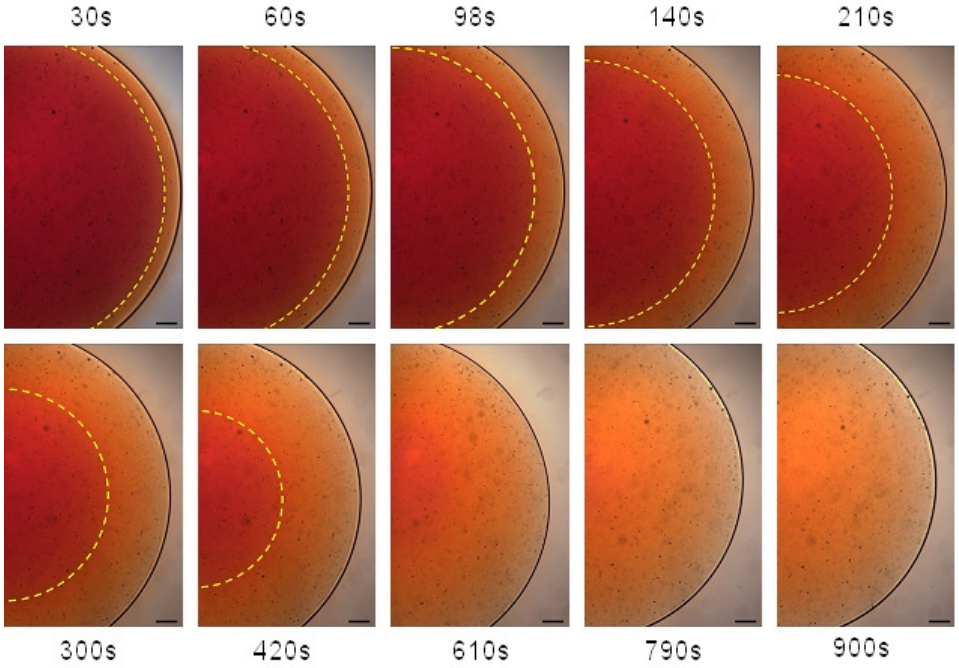

(B)

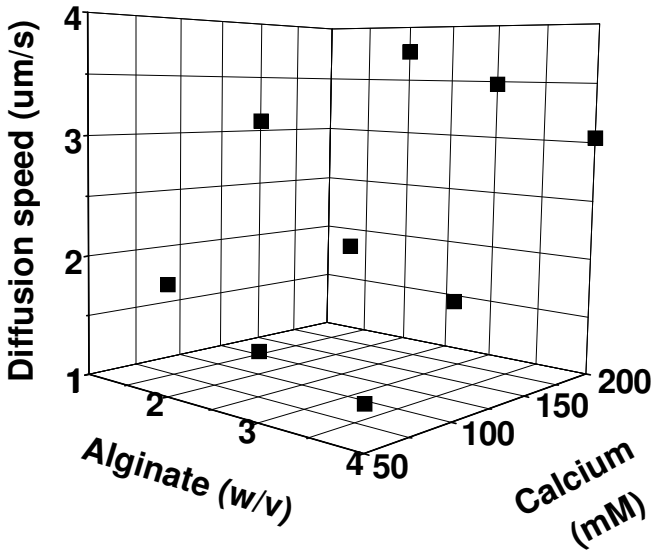

Figure 4.4 Optical images (A) and diffusion speed (B) of calcium ions through alginate droplets. The scale bars are 200 μm.

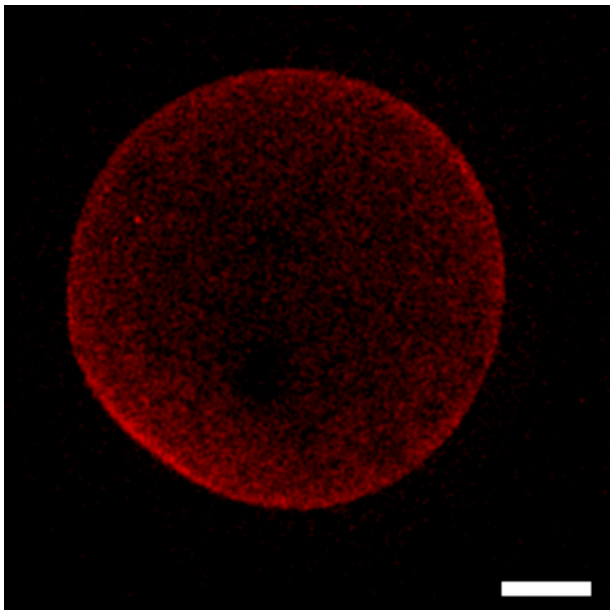

Figure 4.5 A confocal laser scanning microscopic image of an alginate sphere stained with Rhodamine B. The scale bar is 200 μm.

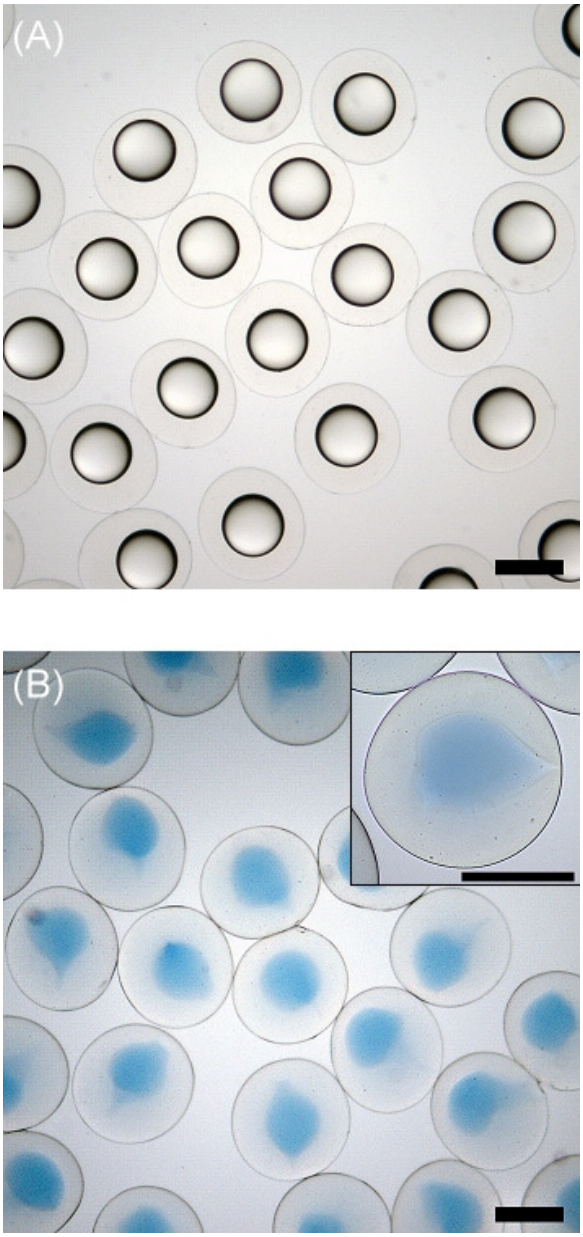

Figure 4.6 Optical microscopic images of alginate spheres encapsulating canola oil (A) and blue dextran (B). The scale bar is 200 μm.

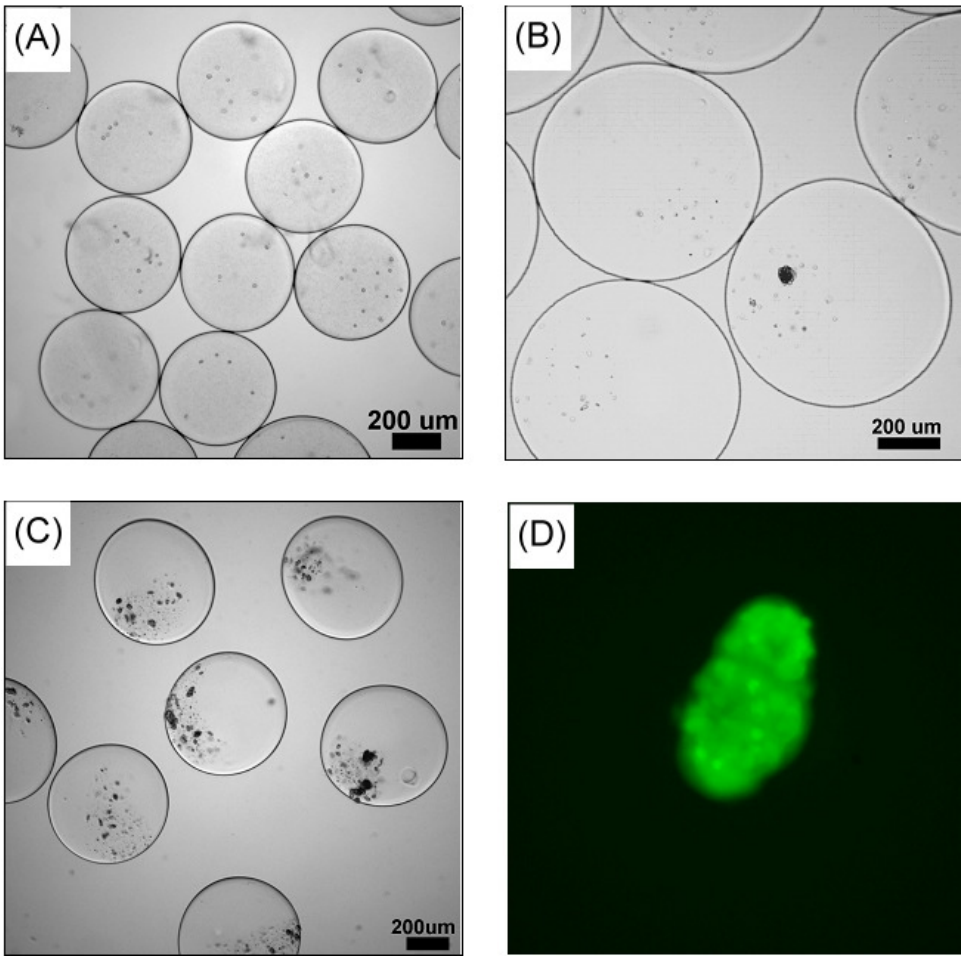

Figure 4.7 Optical images of alginate microcapsules containing mouse fibroblast cells (A), bovine liver tissues (B) and human islet cells (C). A fluorescence optical image of encapsulated islet cells treated with FDA/PI (D).

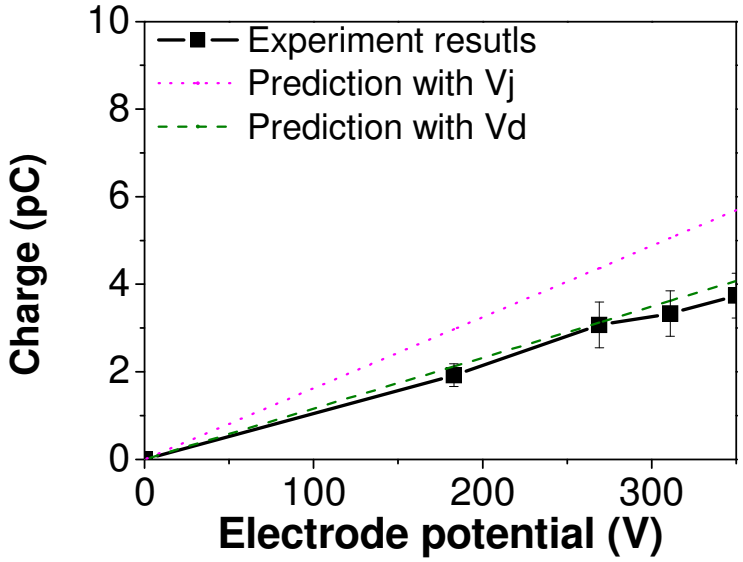

Figure 4.8 Comparison between theoretical and experimental values of induced charge on droplets.

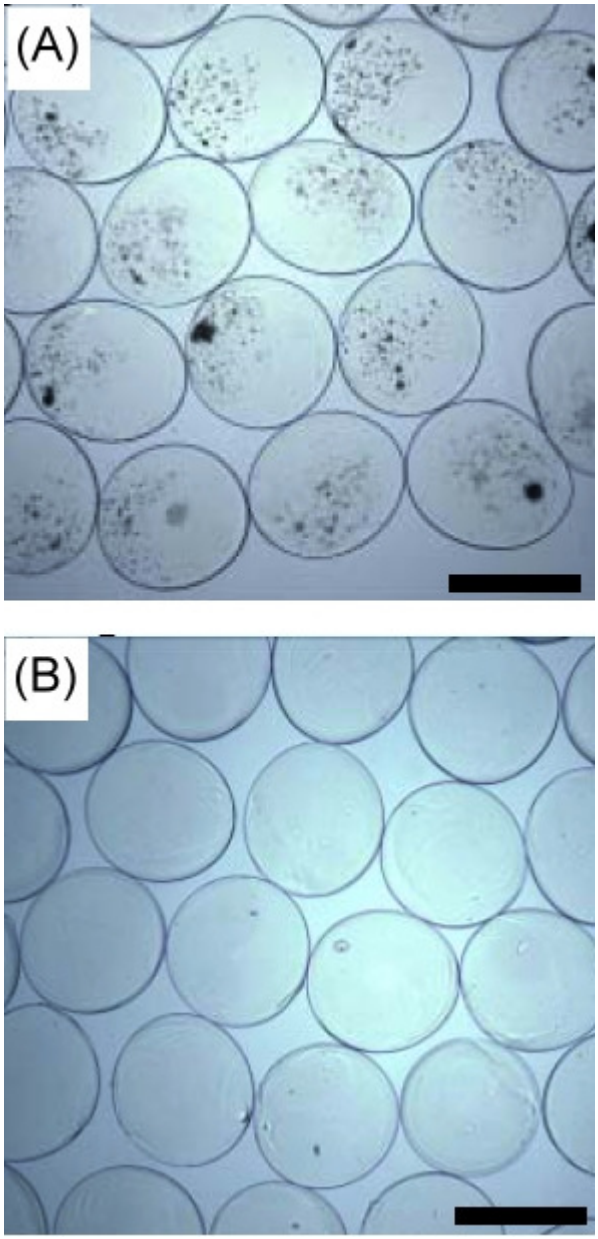

Figure 4.9 Optical images of alginate microcapsules with (A) and without (B) islet cells. The scale bars are 500 μm.

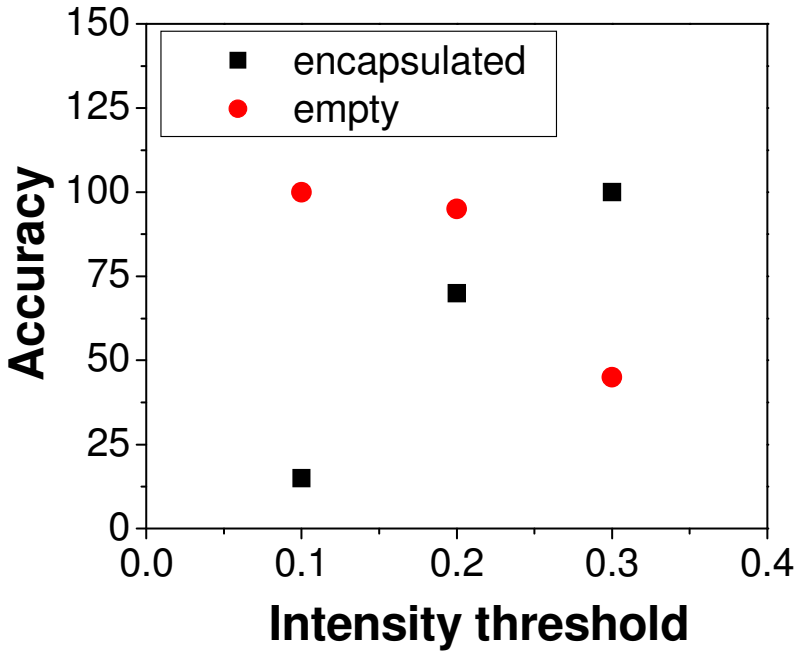

Figure 4.10 Detection accuracy as a function of intensity threshold via light intensity method.

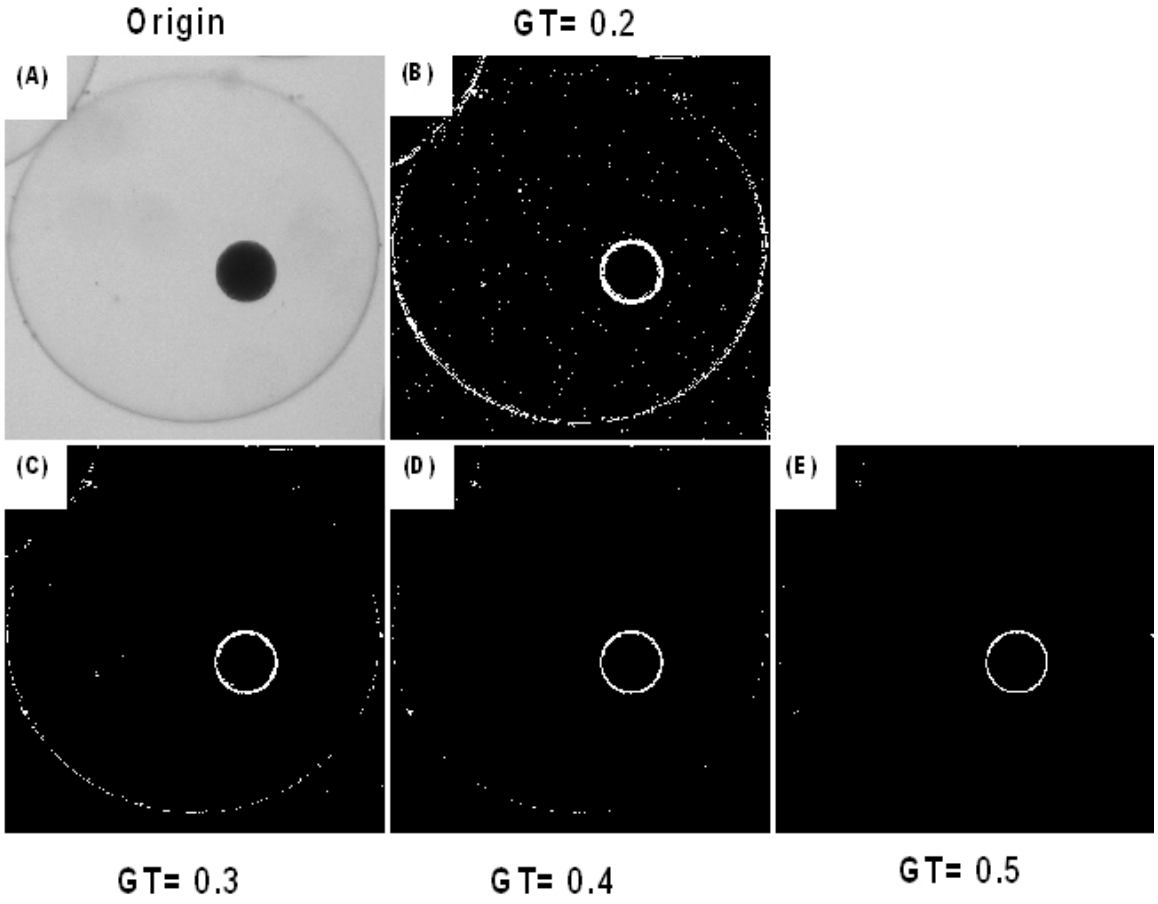

Figure 4.11 Optical images of alginate microcapsules containing ethyl cellulose particles before (A) and after edge detection process (B-E) to show location of edge pixels.

Table 4.1 Overview of some potent applications of encapsulated cells.

Disease	Cell line	Protein
Anyotrophic lateral sclerosis	BHK	CNTF
Diabetes	Langerhans islets	Insulin
Gliomas	293 cells	Endostain
Huntington's disease	BHK	CNTF
Pancreas cancer	293	CYP2B1
Parkinson's disease	PC 12	Dopamine
Chronic pain	Adrenal cells from calves	Catecholamines

CHAPTER 5

CONCLUSIONS AND FUTURE WORK

With increasing availability of potent/delicate drugs such as biomolecules or living cells that are being considered as a therapy, comes the need for developing methods for encapsulating such therapeutics to maintain their functionality/ viability or to increase their delivery specificity. Hydrogel is an excellent candidate as an encapsulation material because of its biocompatibility. On the other hand, fabrication of hydrogel particles may be limited due to the properties of hydrogel and therapeutics and the particle size. In this thesis work, we investigated various applications of uniform hydrogel particles fabricated via precision particle fabrication (PPF) method and its modifications, and we studied the drug release mechanism using a newly formulated model which may help improve the design of drug delivery vehicles.

The gelatin microspheres of precisely controlled size and size distribution, fabricated by the electric field assisted precise particle fabrication (E-PPF) method, allowed a detailed analysis of drug release as a function of glutaraldehyde without the uncertainties related to nonuniformity particle size. Zeta potential measurement showed that higher cross-linking of gelatin led to lower complexation between gelatin and acidic drug. The intraparticle drug distribution patterns indicated that higher complexation of acidic drug took place in the microsphere center as the glutaraldehyde concentration increased, suggesting different affinity to acidic drug within the gelatin microsphere. At

higher glutaraldehyde concentrations, the microsphere surface would be more cross-linked, resulting in higher resistance to degradation and lower gelatin-drug complex. Due to the inhomogeneous cross-linking, the effect of GA concentration on the drug release profile was not linear. The results from this analysis were subsequently used to formulate a release model based on the reaction-diffusion and Michaelis-Menten kinetics. This model accurately predicted the drug release, and was therefore used as a design tool for drug release once the drug diffusion constant and initial drug distribution have been obtained in advance.

For targeted delivery of chemotherapeutics to cancer sites, the gelatin particles were coated with a peptide, eliminating adverse effects resulting from systemic distribution of toxic chemicals. The results of the release study and chemotherapy on cancer cells confirmed that the drug delivery vehicle may substantially enhance the efficacy of chemotherapy which, in turn, would reduce the adverse effect of chemotherapy ascribable to systemic distribution of chemotherapeutics. The drug release from the peptide-coated gelatin particles was triggered by Cathepsin D secreted by the breast cancer cells. Maximization of drug loading could mitigate off-target drug release, and the precise control of the particle size enabled us to obtain the factors affecting the drug loading and drug release, which is not possible with non-uniform particles produced via the conventional methods. Optimal drug loading efficiency could be achieved via basic drug solution (pH=11) and moderate glutaraldehyde concentration (0.0625%) ascribable to the dissociation of the drug in the base and the competition between lower swelling ratio and higher binding between drug and

gelatin as glutaraldehyde concentration increases. To further the study *in vivo*, the electric field strength in the E-PPF method was increased to allow for fabrication of gelatin particles of submicron or nano scale through break-up of the uniform microdroplets. The resulting particles were smaller than 10 μm. A further study is to follow by investigating the optimal particle size for *in vivo* study depending on the clearance rate of particles, release profiles and enhanced permeability and retention effect at the tumor sites. Furthermore, by designing the appropriate peptide sequence specific to different cancer biomarkers, this concept could be expanded to other malignancies.

The PPF method was also modified to encapsulate living cells while maintaining their viability. With this method, alginate microcapsules of different sizes (150-600 μm) were fabricated to allow for encapsulation of various cells, which may advance the development of cell-based therapy. Formation of alginate microspheres/microcapsules from alginate microdroplets involved the motion of both alginate molecules and calcium ions. The significant size shrinkage from alginate microdroplets to microspheres indicated a junction-zone mode of the cross-linking process. A sorting scheme, combining optical detection and electric deflection, was developed to eliminate empty capsules and reduce the net volume of capsules for clinical transplantation. The edge detection method is considered to be more accurate in cell detection compared to the traditional light intensity threshold method.

In conclusion, we have demonstrated versatile application of uniform hydrogel particles in controlled drug delivery and tissue engineering fabricated

via PPF method. The uniform particles of controlled size allowed a more accurate understanding of the drug release mechanism. Drug functionality and cell viability could be maintained after the fabrication/encapsulation process. Continued study with the hydrogel microparticles should lead to more efficacious therapy based on biomolecules and potent therapeutics.

REFERENCES

[1] G. Van den Berghe, A. Wilmer, G. Hermans, W. Meersseman, P.J. Wouters, I. Milants, E. Van Wijngaerden, H. Bobbaers and R. Bouillon, "Intensive insulin therapy in the medical ICU," *New Eng. J. Med.*, vol. 354, pp. 449-461, 2006.

[2] R. Bayston, C.A. Hart and M. Barnicoat, "Intraventricular vancomycin in the treatment of ventriculitis associated with cerebrospinal fluid shunting and drainage," *J. Neurol. Neurosurg. Psychiatry*, vol. 50, pp. 1419-1423, 1987.

[3] P. Petrovic, R. Kalisch, T. Singer and R.J. Dolan, "Oxytocin attenuates affective evaluations of conditioned faces and amygdala activity," *J. Neurosci.*, vol. 28, pp. 6607-6615, 2008.

[4] V. Launay-Vacher, H. Izzedine and G. Deray, "Statins' dosage in patients with renal failure and cyclosporine drug-drug interactions in transplant recipient patients," *Int. J. Cardiol.*, vol. 101, pp. 9-17, 2005.

[5] S. Matsumoto, H. Noguchi, B. Naziruddin, N. Onaca, A. Jackson, N. Hatanaka, T. Okitsu, N. Kobayashi, G. Klintmalm and M. Levy, "Improvement of pancreatic islet cell isolation for transplantation," in *Baylor University Medical Center Proceedings*, 2007, pp. 357-362.

[6] R. Herrero-Vanrell, A.C. Rincon, M. Alonso, V. Reboto, I.T. Molina-Martinez and J.C. Rodriguez-Cabello, "Self-assembled particles of an elastin-like polymer as vehicles for controlled drug release," *J. Control. Release*, vol. 102, pp. 113-122, 2005.

[7] C. Vauthier, C. Dubernet, C. Chauvierre, I. Brigger and P. Couvreur, "Drug delivery to resistant tumors: The potential of poly(alkyl cyanoacrylate) nanoparticles," *J. Control. Release*, vol. 93, pp. 151-160, 2003.

[8] G.M. Barratt, "Therapeutic applications of colloidal drug carriers," *Pharm. Sci. Technol. To.*, vol. 3, pp. 163-171, 2000.

[9] P. Couvreur, C. Dubernet and F. Puisieux, "Controlled drug delivery with nanoparticles: Current possibilities and future trends," *Eur. J. Pharm. Biopharm.*, vol. 41, pp. 2-13, 1995.

[10] G.G. Pitt, M.M. Gratzl, G.L. Kimmel, J. Surles and A. Sohindler, "Aliphatic polyesters II. The degradation of poly (DL-lactide), poly ([epsilon]-caprolactone), and their copolymers in vivo," *Biomaterials*, vol. 2, pp. 215-220, 1981.

[11] G. Orive, R.M. Hernandez, A.R. Gascon, R. Calafiore, T.M.S. Chang, P.D. Vos, G. Hortelano, D. Hunkeler, I. Lacik, A.M.J. Shapiro and J.L. Pedraz, "Cell encapsulation: Promise and progress," *Nat. Med.*, vol. 9, pp. 104-107, 2003.

[12] Y.-S. Hwang, J. Cho, F. Tay, J.Y.Y. Heng, R. Ho, S.G. Kazarian, D.R. Williams, A.R. Boccaccini, J.M. Polak and A. Mantalaris, "The use of murine embryonic stem cells, alginate encapsulation, and rotary microgravity bioreactor in bone tissue engineering," *Biomaterials*, vol. 30, pp. 499-507, 2009.

[13] T.J. Maguire, E.I. Novik, R. Schloss and M.L. Yarmush, "Alginate encapsulation and hepatic differentiation of embryonic stem cells," in *IEEE 31st Annual Northeast Bioengineering Conference*, 2005, pp. 213-214.

[14] A. Joly, J.-F. Desjardins, B. Fremond, M. Desille, J.-P. Campion, Y. Malledant, Y. Lebreton, G. Semana, F. Edwards-Levy, M.-C. Levy and B. Clement, "Survival, proliferation, and functions of porcine hepatocytes encapsulated in coated alginate beads: A step toward a reliable bioartificial liver," *Transplantation*, vol. 63, pp. 795-803, 1997.

[15] S.W. Kim, Y.H. Bae and T. Okano, "Hydrogels: Swelling, drug loading, and release," *Pharmaceut. Res.*, vol. 9, pp. 283-290, 1992.

[16] C. Bienaimé, J.-N. Barbotin and J.-E. Nava-Saucedo, "How to build an adapted and bioactive cell microenvironment? A chemical interaction study of the structure of Ca-alginate matrices and their repercussion on confined cells," *J. Biomed. Mater. Res. A*, vol. 67, pp. 376-388, 2002.

[17] H.L. Kutscher, P. Chao, M. Deshmukh, Y. Singh, P. Hu, L.B. Joseph, D.C. Reimer, S. Stein, D.L. Laskin and P.J. Sinko, "Threshold size for optimal passive pulmonary targeting and retention of rigid microparticles in rats," *J. Control. Release*, vol. 143, pp. 31-37, 2010.

[18] D. Dufrane, R.-M. Goebbels, A. Saliez, Y. Guiot and P. Gianello, "Six-month survival of microencapsulated pig islets and alginate biocompatibility in primates: Proof of concept," *Transplantation*, vol. 81, pp. 1345-1353, 2006.

[19] M. Khalil, A. Shariat-Panahi, R. Tootle, T. Ryder, P. McCloskey, E. Roberts, H. Hodgson and C. Selden, "Human hepatocyte cell lines proliferating as cohesive spheroid colonies in alginate markedly upregulate both synthetic and detoxificatory liver function," *J. Hepatol.*, vol. 34, pp. 68-77, 2001.

[20] P. De Vos, B. De Haan, J. Pater and R. Van Schilfgaarde, "Association between capsule diameter, adequacy of encapsulation, and survival of microencapsulated rat islet allografts," *Transplantation*, vol. 62, pp. 893-899, 1996.

[21] E. Allemann, R. Gurny and E. Doelker, "Preparation of aqueous polymeric nanodispersions by a reversible salting-out process: Influence of process parameters on particle size," *Int. J. Pharm.*, vol. 87, pp. 247-253, 1992.

[22] H. Barbosa, N.K.H. Slater and J.C. Marcos, "Protein quantification in the presence of poly(ethylene glycol) and dextran using the Bradford method," *Anal. Biochem.*, vol. 395, pp. 108-110, 2009.

[23] V. Thongboonkerd, K.R. McLeish, J.M. Arthur and J.B. Klein, "Proteomic analysis of normal human urinary proteins isolated by acetone precipitation or ultracentrifugation," *Kidney Int.*, vol. 62, pp. 1461-1469, 2002.

[24] M.S. Jablonka and P.A. Munro, "Particle size distribution and calcium content of batch-precipitated acid casein curd: Effect of precipitation temperature and pH," *J. Dairy Res.*, vol. 52, pp. 419-428, 1985.

[25] C.J. Coester, K. Langer, H.V. Briesen and J. Kreuter, "Gelatin nanoparticles by two step desolvation--A new preparation method, surface modifications and cell uptake," *J. Microencapsul.*, vol. 17, pp. 187-193, 2000.

[26] A.S. Mujumdar, *Handbook of Industrial Drying*, 3rd ed. Boca Raton, FL: CRC Press, 2006.

[27] G. Orive, S.K. Tam, J.L. Pedraz and J.-P. Hall, "Biocompatibility of alginate-poly-l-lysine microcapsules for cell therapy," *Biomaterials*, vol. 27, pp. 3691-3700, 2006.

[28] K. Iwanaga, T. Yabuta, M. Kakemi, K. Morimoto, Y. Tabata and Y. Ikada, "Usefulness of microspheres composed of gelatin with various cross-linking density," *J. Microencapsul.*, vol. 20, pp. 767-776, 2003.

[29] K. Mitsunaga, T. Yasuhiko, K. Masatoshi, H. Hossein, S. Ayako, F. Ken, M. Masaki, T. Kenji and F. Shingo, "In vivo anti-tumor effect of dual release of cisplatin and adriamycin from biodegradable gelatin hydrogel," *J. Control. Release*, vol. 103, pp. 7-19, 2005.

[30] Y. Tabata and Y. Ikada, "Protein release from gelatin matrices," *Adv. Drug Delivery Rev.*, vol. 31, pp. 287-301, 1998.

[31] Z.S. Patel, M. Yamamoto, H. Ueda, Y. Tabata and A.G. Mikos, "Biodegradable gelatin microparticles as delivery systems for the controlled release of bone morphogenetic protein-2," *Acta Biomaterialia*, vol. 4, pp. 1126-1138, 2008.

[32] O. Taku, Y. Yasumichi, G. Masashi, H. Cheng-Long, N. Tatsuo, S. Yasuhiko, T. Yasuhiko and Y. Hiroyasu, "Slow release of bone morphogenetic protein 2 from a gelatin sponge to promote regeneration of tracheal cartilage in a canine model," *J. Thorac. Cardiov. Sur.*, vol. 127, pp. 329-334, 2004.

[33] M. Yamamoto, Y. Ikada and Y. Tabata, "Controlled release of growth factors based on biodegradation of gelatin hydrogel," *J. Biomater. Sci., Polym. Ed.*, vol. 12, pp. 77-88, 2001.

[34] F.K. Kasper, T. Kushibiki, Y. Kimura, A.G. Mikos and Y. Tabata, "In vivo release of plasmid DNA from composites of oligo(poly(ethylene glycol)fumarate) and cationized gelatin microspheres," *J. Control. Release*, vol. 107, pp. 547-561, 2005.

[35] P. Zarana, U. Hiroki, Y. Masaya, T. Yasuhiko and M. Antonios, "In vitro and in vivo release of vascular endothelial growth factor from gelatin microparticles and biodegradable composite scaffolds," *Pharmaceut. Res.*, vol. 25, pp. 2370-2378, 2008.

[36] A.R. Tzafriri, "Mathematical modeling of diffusion-mediated release from bulk degrading matrices," *J. Control. Release*, vol. 63, pp. 69-79, 2000.

[37] K. Mladenovska, L. Klisarova, E.F. Kumbaradzi, M.G. Dodov, E. Janjevic-Ivanova and K. Goracinova, "Crosslinked gelatin microspheres containing BSA as a vaccine formulation: Biodegradation and drug release control in the presence of trypsin," *B. Chem. Technol. Macedonia*, vol. 20, pp. 151-156, 2001.

[38] T.A. Holland, J.K.V. Tessmar, Y. Tabata and A.G. Mikos, "Transforming growth factor-β1 release from oligo(poly(ethylene glycol) fumarate) hydrogels in conditions that model the cartilage wound healing environment," *J. Control. Release*, vol. 94, pp. 101-114, 2004.

[39] S. Young, M. Wong, Y. Tabata and A.G. Mikos, "Gelatin as a delivery vehicle for the controlled release of bioactive molecules," *J. Control. Release*, vol. 109, pp. 256-274, 2005.

[40] B. Jeong, Y.H. Bae and S.W. Kim, "Drug release from biodegradable injectable thermosensitive hydrogel of PEG-PLGA-PEG triblock copolymers," *J. Control. Release*, vol. 63, pp. 155-163, 2000.

[41] J. Siepmann and N.A. Peppas, "Modeling of drug release from delivery systems based on hydroxypropyl methylcellulose (HPMC)," *Adv. Drug Delivery Rev.*, vol. 48, pp. 139-157, 2001.

[42] C.S. Brazel and N.A. Peppas, "Modeling of drug release from Swellable polymers," *Eur. J. Pharm. Biopharm.*, vol. 49, pp. 47-58, 2000.

[43] H.B. Hopfenberg and H.L. Frisch, "Transport of organic micromolecules in amorphous polymers," *J. Polym. Sci. Pol. Lett.*, vol. 7, pp. 405-409, 1969.

[44] S.N. Rothstein, W.J. Federspiel and S.R. Little, "A unified mathematical model for the prediction of controlled release from surface and bulk eroding polymer matrices," *Biomaterials*, vol. 30, pp. 1657-1664, 2009.

[45] Y. Tabata, Y. Ikada, K. Morimoto, H. Katsumata, T. Yabuta, K. Iwanaga and M. Kakemi, "Surfactant-free preparation of biodegradable hydrogel microspheres for protein release," *J. Bioact. Compat. Polym.*, vol. 14, pp. 371-384, 1999.

[46] Y.B. Choy, F. Cheng, H. Choi and K.K. Kim, "Monodisperse gelatin microspheres as a drug delivery vehicle: Release profile and effect of crosslinking density," *Macromol. Biosci.*, vol. 8, pp. 758-765, 2008.

[47] G.J. Martínez-Díaz, D. Nelson, W.C. Crone and W.J. Kao, "Mechanical and chemical analysis of gelatin-based hydrogel degradation," *Macromol. Chem. Phys.*, vol. 204, pp. 1898-1908, 2003.

[48] D.G. Kanjickal and S.T. Lopina, "Modeling of drug release from polymeric delivery systems--A review," *Crit. Rev. Ther. Drug Carrier Syst.*, vol. 21, pp. 345-386, 2004.

[49] J.M. Berg, J.L. Tymoczko and L. Stryer, *Biochemistry*, 6th ed. New York, NY: W. H. Freeman, 2006.

[50] R.W. Lenz, "Biodegradable polymers," *Adv. Polym. Sci.*, vol. 107, pp. 1-40, 1993.

[51] H.G. Welgus, J.J. Jeffrey and A.Z. Eisen, "The collagen substrate specificity of human skin fibroblast collagenase," *J. Biol. Chem.*, vol. 256, pp. 9511-9515, 1981.

[52] M.E. Stroppolo, M. Falconi, A.M. Caccuri and A. Desideri, "Superefficient enzymes," *Cell. Mol. Life Sci.*, vol. 58, pp. 1451-1460, 2001.

[53] C.M. Ofner and W.A. Bubnis, "Chemical and swelling evaluations of amino group crosslinking in gelatin and modified gelatin matrices," *Pharmaceut. Res.*, vol. 13, pp. 1821-1827, 1996.

[54] A. Bajpai and J. Choubey, "Design of gelatin nanoparticles as swelling controlled delivery system for chloroquine phosphate," *J. Mater. Sci.: Mater. Med.*, vol. 17, pp. 345-358, 2006.

[55] M. Ruiz, A.M. Sastre and E. Guibal, "Palladium sorption on glutaraldehyde-crosslinked chitosan," *React. Funct. Polym.*, vol. 45, pp. 155-173, 2000.

[56] G.C. Fadda, D. Lairez, B. Arrio, J.-P. Carton and V. Larreta-Garde, "Enzyme-catalyzed gel proteolysis: An anomalous diffusion-controlled mechanism," *Biophys. J.*, vol. 85, pp. 2808-2817, 2003.

[57] A. Gabizon and F. Martin, "Polyethylene glycol-coated (pegylated) liposomal doxorubicin. Rationale for use in solid tumours," *Drugs*, vol. 54, pp. 15-21, 1997.

[58] H. Maeda, J. Wu, T. Sawa, Y. Matsumura and K. Hori, "Tumor vascular permeability and the EPR effect in macromolecular therapeutics: A review," *J. Control. Release*, vol. 65, pp. 271-284, 2000.

[59] H. Maeda, "The enhanced permeability and retention (EPR) effect in tumor vasculature: The key role of tumor-selective macromolecular drug targeting," *Adv. Enzyme Regul.*, vol. 41, pp. 189-207, 2001.

[60] A.K. Iyer, G. Khaled, J. Fang and H. Maeda, "Exploiting the enhanced permeability and retention effect for tumor targeting," *Drug Discov. Today*, vol. 11, pp. 812-818, 2006.

[61] L.-Y. Luo, D. Katsaros, A. Scorilas, S. Fracchioli, R. Bellino, M. van Gramberen, H. de Bruijn, A. Henrik, U.-H. Stenman, M. Massobrio, A.G.J. van der Zee, I. Vergote and E.P. Diamandis, "The serum concentration of human kallikrein 10 represents a novel biomarker for ovarian cancer diagnosis and prognosis," *Cancer Res.*, vol. 63, pp. 807-811, 2003.

[62] A.E. Guppy and G.J.S. Rustin, "CA125 response: Can it replace the traditional response criteria in ovarian cancer?" *Oncologist*, vol. 7, pp. 437-443, 2002.

[63] W.J. Catalona, D.S. Smith, T.L. Ratliff, K.M. Dodds, D.E. Coplen, J.J. Yuan, J.A. Petros and G.L. Andriole, "Measurement of prostate-specific antigen in serum as a screening test for prostate cancer," *New Eng. J. Med.*, vol. 324, pp. 1156-1161, 1991.

[64] F. Kosari, Y.W. Asmann, J.C. Cheville and G. Vasmatzis, "Cysteine-rich secretory protein-3: A potential biomarker for prostate cancer," *Cancer Epidemiol. Biomark. Prev.*, vol. 11, pp. 1419-1426, 2002.

[65] B.M. Kacinski, S.K. Chambers, E. Richard Stanley, D. Carter, P. Tseng, K.A. Scata, D.H.Y. Chang, M.H. Pirro, J.T. Nguyen, A. Ariza, L.R. Rohrschneider and V.M. Rothwell, "The cytokine CSF-1 (M-CSF) expressed by endometrial carcinomas in vivo and in vitro, may also be a circulating tumor marker of neoplastic disease activity in endometrial carcinoma patients," *Int. J. Radiat. Oncol. Biol. Phys.*, vol. 19, pp. 619-626, 1990.

[66] M. Ohashi, S. Natori, N. Fujio, H. Iguchi and H. Nawata, "Secretory protein 7B2. A novel tumor marker of medullary carcinoma of the thyroid," *Horm. Metab. Res.*, vol. 22, pp. 114-116, 1990.

[67] L.J. Deftos, "Chromogranin A: Its role in endocrine function and as an endocrine and neuroendocrine tumor marker," *Endocr. Rev.*, vol. 12, pp. 181-188, 1991.

[68] A.K. Tandon, G.M. Clark, G.C. Chamness, J.M. Chirgwin and W.L. McGuire, "Cathepsin D and prognosis in breast cancer," *New Eng. J. Med.*, vol. 322, pp. 297-302, 1990.

[69] N. Ferrara, K.J. Hillan, H.-P. Gerber and W. Novotny, "Discovery and development of bevacizumab, an anti-VEGF antibody for treating cancer," *Nat. Rev. Drug Discov.*, vol. 3, pp. 391-400, 2004.

[70] P. Trail, D. King and G. Dubowchik, "Monoclonal antibody drug immunoconjugates for targeted treatment of cancer," *Cancer Immunol. Immunother.*, vol. 52, pp. 328-337, 2003.

[71] W.-F. Cheng, C.-F. Hung, C.-Y. Chai, K.-F. Hsu, L. He, M. Ling and T.C. Wu, "Tumor-specific immunity and antiangiogenesis generated by a DNA vaccine encoding calreticulin linked to a tumor antigen," *J. Clin. Invest.*, vol. 108, pp. 669-678, 2001.

[72] M.E. Kerman, W.C.W. Chan, P. Laakkonen, S.N. Bhatia and E. Ruoslahti, "Nanocrystal targeting in vivo," *Proc. Natl. Acad. Sci. U. S. A.*, vol. 99, pp. 12617-12621, 2002.

[73] Y.B. Choy, H. Choi and K.K. Kim, "Uniform biodegradable hydrogel microspheres fabricated by a surfactant-free electric-field-assisted method," *Macromol. Biosci.*, vol. 7, pp. 423-428, 2007.

[74] G.T. Hermanson, *Bioconjugation techniques*, 2nd ed. Maryland Heights, MO: Academic Press, Inc., 2008.

[75] S.M. Shafie and L.A. Liotta, "Formation of metastasis by human breast carcinoma cells (MCF-7) in nude mice," *Cancer Lett.*, vol. 11, pp. 81-87, 1980.

[76] B. Kluve, W.C. Merrick, E.J. Stanbridge and H. Gershman, "Mycoplasmas induce collagenase in BALB/c 3T3 cells," *Nature*, vol. 292, pp. 855-857, 1981.

[77] A. Maton, J. Hopkins, C.W. McLaughlin, S. Johnson, M.Q. Warner, D. LaHart and J.D. Wright, *Human Biology and Health.* Boston, MA: Pearson Prentice Hall, 1993.

[78] L. Rayleigh, "On the equilibrium of liquid conducting masses charged with electricity," *Philos. Mag.*, vol. 14, pp. 184-186, 1882.

[79] F. Lim and A.M. Sun, "Microencapsulated islets as bioartificial endocrine pancreas," *Science*, vol. 210, pp. 908-910, 1980.

[80] S.-P. Kim, D.-H. Lee and J.-K. Park, "Development of hepatocyte spheroids immobilization technique using alternative encapsulation method," *Biotechnol. Bioprocess Eng.*, vol. 3, pp. 96-102, 1998.

[81] T. Visted, R. Bjerkvig and P.Ø. Enger, "Cell encapsulation technology as a therapeutic strategy for CNS malignancies," *Neuro-Oncology*, vol. 3, pp. 201-210, 2001.

[82] T. Wang, I. Lacik, M. Brissova, A.V. Anilkumar, A. Prokop, D. Hunkeler, R. Green, K. Shahrokhi and A.C. Powers, "An encapsulation system for the immunoisolation of pancreatic islets," *Nat. Biotechnol.*, vol. 15, pp. 358-362, 1997.

[83] W.-G. Koh, A. Revzin and M.V. Pishko, "Poly(ethylene glycol) hydrogel microstructures encapsulating living cells," *Langmuir*, vol. 18, pp. 2459-2462, 2002.

[84] A. Khademhosseini, G. Eng, J. Yeh, J. Fukuda, J. Blumling, R. Langer and J.A. Burdick, "Micromolding of photocrosslinkable hyaluronic acid for cell encapsulation and entrapment," *J. Biomed. Mater. Res. A*, vol. 79A, pp. 522-532, 2006.

[85] K.H. Bae, J.J. Yoon and T.G. Park, "Fabrication of hyaluronic acid hydrogel beads for cell encapsulation," *Biotechnol. Prog.*, vol. 22, pp. 297-302, 2006.

[86] B. A. Zielinski and P. Aebischer, "Chitosan as a matrix for mammalian cell encapsulation," *Biomaterials*, vol. 15, pp. 1049-1056, 1994.

[87] H. Gin, B. Dupuy, C. Baquey, D. Ducassou and J. Aurertin, "Agarose encapsulation of islets of Langerhans: Reduced toxicity in vitro," *J. Microencapsul.*, vol. 4, pp. 239-242, 2008.

[88] K. Potter, B.J. Balcom, T.A. Carpenter and L.D. Hall, "The gelation of sodium alginate with calcium ions studied by magnetic resonance imaging (MRI)," *Carbohydr. Res.*, vol. 257, pp. 117-126, 1994.

[89] B. Thu, P. Bruheim, T. Espevik, O. Smidsrød, P. Soon-Shiongb and G. Skjåk-Bræk, "Alginate polycation microcapsules II. Some functional properties," *Biomaterials*, vol. 17, pp. 1069-1079, 1996.

[90] A. Degrassi, R. Toffanin, S. Paoletti and L.D. Hall, "A better understanding of the properties of alginate solutions and gels by quantitative magnetic resonance imaging (MRI)," *Carbohydr. Res.*, vol. 306, pp. 19-26, 1998.

[91] G. Fundueanu, C. Nastruzzi, A. Carpov, J. Desbrieres and M. Rinaudo, "Physico-chemical characterization of Ca-alginate microparticles produced with different methods," *Biomaterials*, vol. 20, pp. 1427-1435, 1999.

[92] J.-M. Duez, M. Mestdagh, R. Demeure, J.-F. Goudemant, B.P. Hills and J. Godward, "NMR studies of calcium-induced alginate gelation. Part I—MRI tests of gelation models," *Magn. Reson. Chem.*, vol. 38, pp. 324-330, 2000.

[93] B. Thu, O. Gaserod, D. Paus, A. Mikkelsen, G. Skjåk-Bræk, R. Toffanin, F. Vittur and R. Rizzo, "Inhomogeneous alginate gel spheres: An assessment of the polymer gradients by synchrotron radiation-induced X-ray emission, magnetic resonance microimaging, and mathematical modeling," *Biopolymers*, vol. 53, pp. 60-71, 2000.

[94] Y.A. Morch, I. Donati and B.L. Strand, "Effect of Ca2+, Ba2+, and Sr2+ on alginate microbeads," *Biomacromolecules*, vol. 7, pp. 1471-1480, 2006.

[95] L. Li, Y. Fang, R. Vreeker, I. Appelqvist and E. Mendes, "Reexamining the egg-box model in calcium-alginate gels with X-ray diffraction," *Biomacromolecules*, vol. 8, pp. 464-468, 2007.

[96] M. Otterlei, K. Ostgaard, G. Skjak-Braek, O. Smidsrod, P. Soon-Shiong and T. Espevik, "Induction of cytokine production from human monocytes stimulated with alginate," *J. Immunother.*, vol. 10, pp. 286-291, 1991.

[97] B. Kulseng, G. Skjak-Braek, L. Ryan, A. Andersson, A. King, A. Faxvaag and T. Espevik, "Transplanation of alginate microcapsules: Generation of antibodies against alginates and encapsulated porcine islet-like cell clusters," *Transplantation*, vol. 67, pp. 978-984, 1999.

[98] M.G. Levee, G.-M. Lee, S.-H. Paek and B.O. Palsson, "Microencapsulated human bone marrow cultures: A potential culture system for the clonal outgrowth of hematopoietic progenitor cells," *Biotechnol. Bioeng.*, vol. 43, pp. 734-739, 1994.

[99] B. Bugarski, J. Smith, J. Wu and M.F.A. Goosen, "Methods for animal cell immobilization using electrostatic droplet generation," *Biotechnol. Tech.*, vol. 7, pp. 677-682, 1993.

[100] U. Prube, B. Fox, M. Kirchhoff, F. Bruske, J. Breford and K.-D. Vorlop, "New process (jet cutting method) for the production of spherical beads from highly viscous polymer solutions," *Chem. Eng. Technol.*, vol. 21, pp. 29-33, 1998.

[101] H. Brandenberger and F. Widmer, "A new multinozzle encapsulation/immobilisation system to produce uniform beads of alginate," *J. Biotechnol.*, vol. 63, pp. 73-80, 1998.

[102] H. Zimmermann, S. Shirley and U. Zimmermann, "Alginate-based encapsulation of cells: Past, present, and future," *Curr. Diab. Rep.*, vol. 7, pp. 314-320, 2007.

[103] B.L. Strand, O. Gåserød, B. Kulseng, T. Espevik and G. Skjåk-Bræk, "Alginate-polylysine-alginate microcapsules: Effect of size reduction on capsule properties," *J. Microencapsul.*, vol. 19, pp. 615-630, 2002.

[104] K.H. Jones and J.A. Senft, "An improved method to determine cell viability by simultaneous staining with fluorescein diacetate-propidium iodide," *J. Histochem. Cytochem.*, vol. 33, pp. 77-79, 1985.

[105] H.M. Shapiro, *Practical flow cytometry*, 3rd ed. New York, NY: Wiley-Liss, 2005.

[106] O. Reynolds, "An experimental investigation of the circumstances which determine whether the motion of water shall be direct or sinuous, and of the law of resistance in parallel channels," *Philosophical Transactions of the Royal Society*, vol. 174, pp. 935-982, 1883.

[107] H. Uludag, P. De Vos and P.A. Tresco, "Technology of mammalian cell encapsulation," *Adv. Drug Delivery Rev.*, vol. 42, pp. 29-64, 2000.

[108] N.E. Simpson, C.L. Stabler, C.P. Simpson, A. Sambanis and I. Constantinidis, "The role of the CaCl2-guluronic acid interaction on alginate encapsulated β TC3 cells," *Biomaterials*, vol. 25, pp. 2603-2610, 2004.

[109] G. Orive, R.M. Hernández, A.R. Gascón and J.L. Pedraz, Biomedical applications of immobilized cells, Immobilization of Enzymes and Cells, 2006, pp. 427-437.

AUTHOR'S BIOGRAPHY

Felice Cheng was born in Hsinchu County, Taiwan, on September 20, 1981. She received the BS and MS degrees (2003 and 2004, respectively) in Electronics Engineering at Chiao-Tung University. She received the Ph.D. degree in Electrical and Computer Engineering from the University of Illinois at Urbana-Champaign (UIUC) in 2010.

Her research at Chiao-Tung University was on a low power implantable integrated chip with solar cells for artificial retinal prostheses. She was a teaching assistant in digital signal processing at UIUC in fall 2009. She conducted research on fabrication of biocompatible hydrogels for advanced drug delivery systems and cell encapsulation at UIUC.